OUKA
The University of Osaka
Institutional Knowledge Archive

Title	Molecular orientation analysis in organic transistor devices by polarization dependent and low-frequency Raman spectroscopy
Author(s)	Bhardwaj, Bishwajeet Singh
Citation	大阪大学, 2020, 博士論文
Version Type	VoR
URL	https://doi.org/10.18910/76527
rights	
Note	

The University of Osaka Institutional Knowledge Archive : OUKA

https://ir.library.osaka-u.ac.jp/

The University of Osaka

Doctoral Dissertation

Molecular orientation analysis in organic transistor devices by polarization dependent and low-frequency Raman spectroscopy

Bishwajeet Singh Bhardwaj

December 2019

Graduate School of Engineering,

Osaka University

Table of contents

Introduction 3

Chapter 1. Polarization dependent Raman spectroscopy 6

1.1 Fundamentals of Raman scattering 6

1.2 Fundamental of polarization dependent Raman spectroscopy 17

1.3 Application of polarization dependent Raman spectroscopy 20

Chapter 2. Raman spectrum calculation by density functional theory (DFT) 26

2.1 Electronic structure calculation by DFT 26

2.2 Calculation of molecular normal modes in Gaussian 30

2.3 Calculation of Raman scattering in Gaussian 32

Chapter 3. Organic field effect transistor devices (OFET) 37

3.1 Introduction of OFET devices 37

3.2 Output characteristics of OFET 38

3.3 Application of OFET devices 42

Chapter 4. Molecular orientation analysis of pentacene in OFET device by polarization dependent Raman spectroscopy 46

4.1 Introduction of organic semiconductor molecule pentacene 46

4.2 Fabrication method and electronic characteristics of the transistor device 47

4.3 Analysis of molecular orientation of pentacene in transistor devices 51

Chapter 5. Raman spectroscopic investigations of dinaphthothienothiophene (DNTT) 64

5.1 Introduction of DNTT molecule 64

5.2 Fabrication of transistor device based on DNTT 65

5.3 Raman spectroscopic analysis of DNTT in a transistor device 67

Chapter 6. Investigation of the intermolecular interactions of dinaphthothienothiophene (DNTT) molecules in a transistor device by low-frequency Raman spectroscopy 79

6.1 Introduction of low-frequency Raman spectroscopy 79

6.2 Experimental setup for low-frequency Raman spectroscopy 82

6.3 Investigation of intermolecular interactions of DNTT in a transistor device 84

Conclusions 89

List of publications 91

Acknowledgements 93

Introduction

Nowadays, organic semiconducting materials are used in many electronic devices such as flexible display, electronic skin, plastic circuits, non-volatile plastic memories, and sensors. These applications are possible due to the lightweight and flexible properties of the organic materials. Among various organic materials, the application of pentacene and dinaphthothienothiophene (DNTT) has recently increased because of their high charge carrier mobility in organic field-effect transistor (OFET) devices. The structural properties of these organic materials, such as the molecular orientation and molecular density distribution, have a significant impact on their charge carrier mobility in the transistor devices, therefore investigating these properties is essential. Raman spectroscopy is known as a promising technique that can study the structural properties of organic materials with a high spatial resolution.

In my research, I studied the molecular orientation of pentacene in real transistor devices using polarization-dependent Raman spectroscopy. The presence of impurities in pentacene molecules changes the alignments of pentacene and hence, affects the transport of charge carriers in the device. Sublimation is a well-known process to remove these impurities. In this dissertation, I mapped the variation of tilt orientation between neighboring measurement positions that are separated by a distance of a few hundreds of nanometers in devices fabricated utilizing non-sublimated and sublimated pentacene, which can be directly correlated to the device performance and can help in improving performances of electronic devices.

I also investigated Raman spectroscopic studies on the DNTT molecule in a real transistor device for the first time. I observed that the Raman spectrum of the DNTT contains several vibrational modes. I performed a density functional theory (DFT) calculation on the DNTT molecule, which helped me in describing the nature of vibrations of all observed Raman modes of the DNTT molecule. I investigated the density distribution and orientations of this molecule in the device using Raman spectroscopy. This study can be utilized in improving performances of electronic devices made of DNTT molecules.

Further, I studied the intermolecular interactions of DNTT molecules in the transistor device using the low-frequency Raman spectroscopy. I used several Bragg notch filters in the optical path to detect low-frequency Raman signals. I found out that DNTT molecules clearly show a few low-frequency Raman modes for the first time. I further investigated the spatial variation of intermolecular interactions, i.e., the molecular packing of DNTT molecules in the device using a low-frequency Raman imaging. This work helped me to identify the regions of the device that could have high carrier mobility with a high spatial resolution. This information could be utilized in designing high performing transistor devices.

In Chapter 1 of my dissertation, I will discuss the fundamentals of the Raman scattering, the polarization-dependent Raman scattering, and then the application of polarization-dependent Raman spectroscopy technique.

In Chapter 2, the calculation of the electronic structure by density functional theory (DFT) will be introduced. Then, the calculation of normal vibrational frequency and calculation of the Raman spectrum by DFT will be described in this chapter.

In Chapter 3, the introduction and output characteristics of the transistor devices will be discussed along with the applications of the OFET devices.

In Chapter 4, I will first introduce the pentacene molecule, after which the fabrication method and the output characteristics of the fabricated transistor device will be discussed. Later on, I will discuss about the analysis of the orientation distribution of pentacene in transistor devices using polarization-dependent Raman spectroscopy.

In Chapter 5, my work on Raman spectroscopic studies of DNTT in the transistor device will be discussed. I will describe the structure and properties of the DNTT molecule and the fabrication of DNTT based transistor device in detail. Then, I will explain the Raman spectroscopic analysis of DNTT molecules using DFT calculation. I will also discuss the investigation of the orientation of DNTT molecules in the device using polarization-dependent Raman spectroscopy.

In Chapter 6, I will discuss my work on the investigation of the intermolecular interactions of DNTT molecules in the device by low-frequency Raman spectroscopy. I will introduce low-frequency Raman spectroscopy and then, I will discuss about the optical set-up for measuring low-frequency Raman modes. Later, I will discuss on the investigation of intermolecular interactions of DNTT molecules using Raman imaging in the device.

Finally, I will give conclusions of my research work.

Chapter 1. Polarization dependent Raman spectroscopy

1.1 Fundamentals of Raman scattering

Raman scattering occurs as a result of the interaction of light with a material, and there is an exchange of energy between them.[1-4] As this process involves energy transfer between light and material, it is utilized to study various chemical and physical properties of the material and finds a number of practical applications in several fields including physics, chemistry, material science, biology, and medicine.[5-7]

As we know that a photon is the fundamental particle of light or electromagnetic radiation. When light interacts with the molecules, it causes photons and electrons to move, which induces an oscillating dipole within the molecules.[8-10] The induced oscillating dipole moment is manifested as a source of light, which results in the scattering of light. A large number of scattered photons emit at a similar frequency (ω_0) as that of the incident light, and the process referred to an elastic scattering, which is known as the Rayleigh scattering of light. On the other hand, there is also additional light scattering occurs at the different frequencies of the incident light due to the energy exchange among photons and molecules, which is known as an inelastic scattering of light and the Raman scattering is an example of this scattering. In the elastic scattering of light, the value of scattered frequency can be shifted by "ω_1" towards the lower or higher frequency region by gaining energy or losing energy to the molecules. When the incoming light gains energy from molecules, the energy of scattered light becomes "$\omega_0 + \omega_1$" and this process referred to as anti-stokes Raman scattering. In another case,

when the incoming light loses energy to molecules, the energy of scattered light becomes "$\omega_0 - \omega_1$" and this process referred to as the Stokes Raman scattering. The process of anti-Stokes Raman scattering, Rayleigh scattering, and stokes Raman scattering are schematically represented in Fig. 1-1.

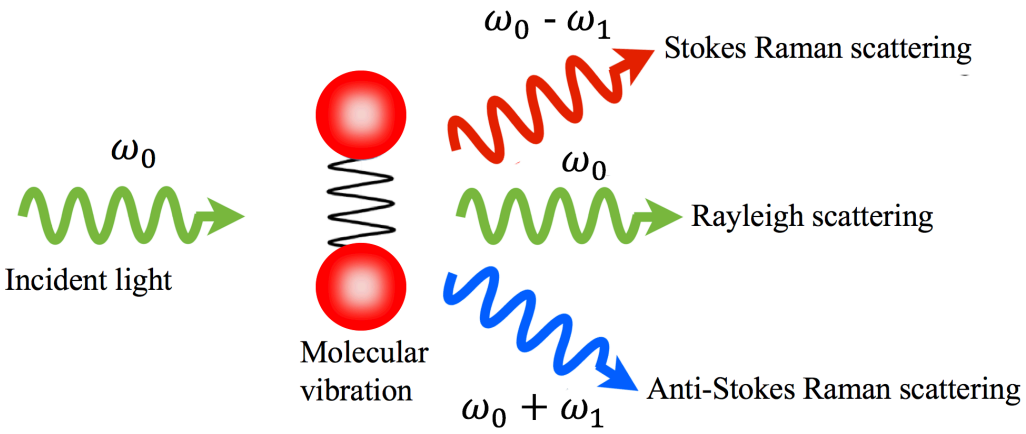


Figure 1-1 shows the Stokes, Rayleigh, and anti-Stokes Raman scattering at frequency $\omega_0 - \omega_1$, ω_0, and $\omega_0 + \omega_1$, respectively.

In the Raman scattering, the scattered light has different frequencies than that of the incident light. Raman scattering of light was first theoretically described by Smekal[11] in 1923 and first experimentally observed by Raman[12] in 1928. As the frequency shift represents the energy level of the molecule scattering the incident light, one can extract rich information of the molecular bonds by detecting Raman scattered photons from the molecules[13]. Moreover, owing to the property of visible light, Raman spectroscopy allows observing a sample nondestructively. Therefore, it finds a number

of applications in the field of material science, electric physics, bioscience, and medicine.[14- 18]

In order to understand the Raman scattering, two theories, classical theory and quantum theory, are most often used. The classical theory considers the wave nature of light, which does not consider about the quantized nature of the vibration. However, the quantum theory of Raman scattering takes account of the quantized nature of light.

Classical theory of Raman scattering

In this section, I discuss about the theory of the Raman scattering[19] in which both the material system and incident electromagnetic radiation are treated classically.[20,21] The interaction of a photon with molecule results in the movement of electron and photon, which induces an oscillating dipole inside the molecule. As the Raman scattering occurs at different frequencies than the frequency of incident light, the induced dipole radiates photons with different frequencies.

A dipole moment was induced by the incident electromagnetic wave during the light-matter interaction. The strength of the dipole moment (P) is explained in terms of an electric field of the incident light.[22]

$$P = \alpha E \tag{1.1}$$

Where E denotes the strength of the electric field and α as the polarizability of material that depends on its molecular structure.

The electric field of the incident electromagnetic field is written as follows.[23]

$$E = E_0 \cos(2\pi\, \omega_0 t) \tag{1.2}$$

Where ω_0 denotes frequency of the incident light. Substitution of equation (1.2) into (1.1) results in a time-dependent induced dipole moment as written below.[23]

$$P = \alpha E_0 \cos(2\pi\, \omega_0 t) \tag{1.3}$$

The relative positions of individual atoms in a molecule determine the local electron cloud of the molecular structure, which follows polarizability of the molecule as a function of the instantaneous location of individual atoms. The individual atoms in the molecule are confined to specific vibration modes for any molecular bond, which is cyclical. If Q_0 represents the maximum physical displacement of atom about the equilibrium position, the physical displacements of atoms, $dQ,$ about their equilibrium position in a molecule due to a specific vibration mode can be written in terms of frequency of the vibrational mode (ω_{vib}) as follows.[23]

$$dQ = Q_0 co\, s(2\pi\omega_{vib} t) \tag{1.4}$$

For a very small displacement, Taylor series can be utilized to approximate the polarizability as shown in equation (1.5).[23]

$$\alpha = \alpha_0 + \frac{\partial \alpha}{\partial Q} dQ \tag{1.5}$$

Where α_0 denotes polarizability of the molecule at the equilibrium position. Now, using vibration displacement of the equation(1.4), the polarizability can be written as below.[23]

$$\alpha = \alpha_0 + \frac{\partial \alpha}{\partial Q} Q_0 cos(2\pi\omega_{vib} t) \tag{1.6}$$

Finally, Equation (1.5) is substituted in equation (1.6), results in the below equation. [23]

$$P = \alpha_0 E_0 cos(2\pi\omega_0 t) + \frac{\partial \alpha}{\partial Q} Q_0 E_0 cos(2\pi\omega_0 t)\, cos(2\pi\omega_{vib} t) \tag{1.7}$$

Using a trigonometric identity, Equation (1.7) can be written as below equation.[23]

$$P = \alpha_0 E_0 cos(2\pi\omega_0 t) + \left[\frac{\partial \alpha}{\partial Q} \frac{Q_0 E_0}{2}\right] \{\cos[2\pi(\omega_0 - \omega_{vib})t] + \cos[2\pi(\omega_0 + \omega_{vib})t]\} \tag{1.8}$$

From the above equation (1.8), we understand that the induced dipole moment is created at three distinct frequencies, namely ω_0, $\omega_0-\omega_{vib}$, and $\omega_0+\omega_{vib}$ that results in the scattering of photon with the same three frequencies. The first scattered frequency (ω_0) has the same frequency as that of the incident light, hence it is the case of elastic, i.e., the Rayleigh scattering of light. On the other hand, the latter two frequencies in equation (1.8) that are shifted to higher ($\omega_0+\omega_{vib}$) and lower ($\omega_0-\omega_{vib}$) frequencies are a result of the inelastic scattering of light. The scattering of light in these two cases is termed as the Stokes Raman scattering with higher shifted, and the anti-Stokes Raman scattering with lower shifted frequencies. From the above equation, the essential condition for the Raman scattering is that the term $^{\partial\alpha}/_{\partial Q}$ must be a non-zero quantity, which means that the vibrational displacement of atoms in a molecule corresponding to a specific vibrational mode must show a change in the polarizability.

The classical theory explains the correct dependence of frequency for the Rayleigh and Raman scattering with some limitations. As classical theory does not describe the discrete rotational frequencies of molecules, it cannot be applied to the molecular rotations. When quantum mechanics is used describing the molecular vibrations, the classical amplitude 'Q' is replaced by a quantum mechanical amplitude. The complete treatment of all aspects of the Raman scattering can be understood by understanding the quantum mechanical theory.

Quantum Mechanical Theory of Raman Scattering

Quantum mechanical consideration of both the mechanical system and the incident electromagnetic radiation leads to a different approach to the theory of Raman scattering that is explained here. The incident photon acts as the source of a time-dependent perturbation on molecular energy levels, and the scattering from the molecule is interpreted by this perturbation. To quantify this scattering, first, consider a system without any incident photon interacting with the molecule. In this case, the Schrödinger equation of an unperturbed time-dependent wave function is expressed as below.[23]

$$\mathcal{H}^0\Psi_k^0(q,t) = -\frac{\hbar}{i}\frac{\partial}{\partial t}\Psi_k^0(q,t) \tag{1.9}$$

where $\mathcal{H}^0$ denotes the Hamiltonian and $\Psi_k^0(q,t)$ denotes the wave function with 'q' as the coordinate, and 't' as the time of the system before its interaction with light wave.

The general solution of Eq.(1.9) is solved by introducing functions that depend only on coordinates and time, which could be described as follows.[23]

$$\Psi_k^0(q,t) = \Psi_k(q)\,\varphi_k(t) \tag{1.10}$$

The components of the wave function as function of coordinate and time, are denoted by $\Psi_k(q)$ and $\varphi_k(t)$, respectively. Therefore, solution of the equation (1.10) can be expressed as below.[23]

$$\Psi_k^0(q,t) = \Psi_k(q) e^{\frac{-i}{\hbar} W_k t} \tag{1.11}$$

Where W_k denotes the specific value of the energy of the state k. In the process of interaction of an incident photon with the molecular system, the external electric field generates a potential at the place of the electrons in molecules. Hence, by considering perturbation potential, $\mathcal{H}^1$, the Schrödinger equation is described by the below equation.[23]

$$(\mathcal{H}^0 + \mathcal{H}^1)\,\Psi_k(q,t) = -\frac{\hbar}{i}\frac{\partial}{\partial t}\Psi_k(q,t) \tag{1.12}$$

$\mathcal{H}^1 = -ME$, and $M = \sum_j e_j r_j$,electric charge of the j^{th} electron is denoted by e_j and the momentum induced in the molecules as r_j. In the calculations of the first order, the wave function $\Psi_k(q,t)$ for a state k is expressed as below.[23]

$$\Psi_k(q,t) = \Psi_k^0(q,t) + \Psi_k^1(q,t) \tag{1.13}$$

The electric field, E, is described by the below equation.[23]

$$E = A^* \exp(2\pi\omega_0 t) + Aexp(-2\pi\omega_0 t) \quad (1.14)$$

where A is a complex vector (A = a+ib), and ω_0 denotes the frequency of incident light. The solution of equation (1.13) is expressed in the form of below.[23]

$$\Psi_k^1(q,t) = \Psi_k^+(q)e^{\frac{-i}{\hbar}(W_k+h\omega_0)t} + \Psi_k^-(q)e^{\frac{-i}{\hbar}(W_k-h\omega_0)t} \quad (1.15)$$

Therefore, by substituting the above equation (1.15) in equation (1.13), we can determine $\Psi_k^+(q)$ and $\Psi_k^-(q)$ in terms of the unperturbed system Ψ_r as written below.[23]

$$\Psi_k^+(q) = \sum_r \frac{(AM_{kr})}{W_r - W_k - \omega_0}\Psi_r \quad (1.16)$$

$$\Psi_k^-(q) = \sum_r \frac{(A^*M_{kr})}{W_r - W_k + \omega_0}\Psi_r \quad (1.17)$$

Then, the solution of equation (1.13) is expressed as below.[23]

$$\Psi_k^1(q,t) = \frac{1}{h}\sum_r \Psi_r[\frac{(AM_{kr})}{\omega_{rk} - \omega_0}e^{\frac{-i}{\hbar}(W_k+h\omega_0)t} + \frac{(A^*M_{kr})}{\omega_{rk} + \omega_0}e^{\frac{-i}{\hbar}(W_k-h\omega_0)t}] \quad (1.18)$$

$$\boldsymbol{M}_{kn} = \int (\Psi_k^0(q,t) + \Psi_k^1(q,t))^* \boldsymbol{M}\left(\Psi_k^0(q,t) + \Psi_k^1(q,t)\right)d\tau \quad (1.19)$$

Here, $h\omega_{rk}$ denotes the energy difference between state k and r; $W_r - W_k$. The vector $\boldsymbol{M}_{kn}$ denotes an electronic dipole matrix element of transitions between the states k and n.

By substituting equation (1.18) and an identical expression for a complex conjugate wave function $\Psi_k^1(q,t)^*$ in equation (1.19), the moment of the state k is written as below.[23]

$$\boldsymbol{M}_{kk} = M_{kk}^0 + \frac{1}{h}\sum_r \left[\frac{(AM_{kr})M_{rk}}{\omega_{rk}-\omega_0} + \frac{M_{kr}(AM_{kr})}{\omega_{rk}+\omega_0}\right] e^{-2\pi i\omega_0 t} + \frac{1}{h}\sum_r \left[\frac{(A^*M_{kr})M_{rk}}{\omega_{rk}-\omega_0} + \frac{M_{kr}(AM_{kr})}{\omega_{rk}+\omega_0}\right] e^{2\pi i\omega_0 t} \quad (1.20)$$

In equation (1.20), the first part of the right-hand side of the equation is not dependent on time as well as not associated with radiation, which indicates a permanent moment of the molecule. The second and third parts indicate component oscillation at the same frequency with the frequency of incident light, and therefore, represent dipole oscillation radiating Rayleigh scattering light. Similarly, the following expression about the electric dipole matrix element (M_{kn}) for the transition between the states k and n are calculated.[23]

$$\boldsymbol{M}_{kn} = M_{kn}^0 + M_{kn}^1 + M_{kn}^2$$

$$\boldsymbol{M}_{kn}^0 = \boldsymbol{M}_{kn} e^{-2\pi i\omega_0 t} \quad (1.21)$$

$$M_{kn}^{1} = \frac{1}{h}\sum_{r}\left[\frac{(AM_{kr})M_{rn}}{\omega_{rk}-\omega_{0}} + \frac{M_{kr}(AM_{rn})}{\omega_{rn}+\omega_{0}}\right]e^{-2\pi i(\omega_{kn}+\omega_{0})t} + \frac{1}{h}\sum_{r}\left[\frac{(A^{*}M_{kp})M_{rn}}{\omega_{rk}-\omega_{0}} + \frac{M_{kr}(A^{*}M_{rn})}{\omega_{rn}+\omega_{0}}\right]e^{-2\pi i v_{0}(\omega_{kn}-\omega_{0})t} \quad (1.22)$$

Equation (1.21) describes the electric dipole oscillating at frequency ω_{kn}. Hence, $\boldsymbol{M}_{kn}^{0}$ corresponds to the absorption or emission of radiation ($\omega_0 = \omega_{kn}$). Equation 1.22 represents the electric dipole oscillating at the frequency $\omega_0 + \omega_{kn}$ and $\omega_0 - \omega_{kn}$ and M_{kn}^{1} is the component related to the Raman scattering. Figure 1-2 illustrates the energy diagram for the different scattering processes.

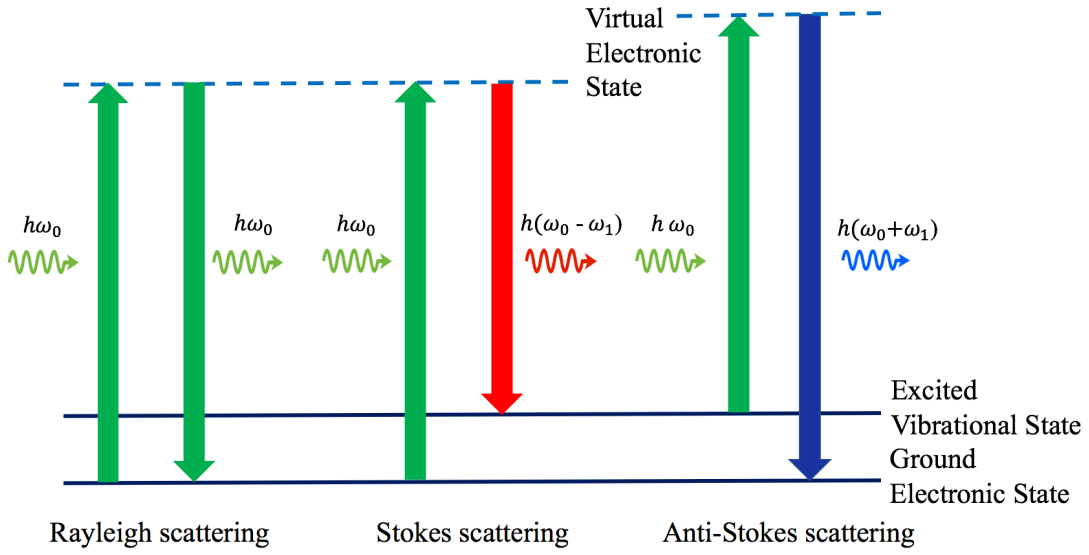


Figure 1-2. shows the excitation and scattering mechanism in molecules.

1.2 Fundamental of polarization dependent Raman spectroscopy

The effect of Raman scattering takes place in the molecular structure when the light irradiant on the molecule instigates molecular vibration. The intensity of Raman scattering is dependent on the interaction between the polarization of excitation light and the direction of molecular vibration. When the light irradiates on a molecule oscillated in a specific direction, the polarization of light in that specific direction interacts with the molecule. The more the interaction between them, there would be higher the intensity of Raman scattering. As the intensity of the Raman scattered light is sensitive to the polarization of the light irradiant on the molecule, the polarization-dependent Raman spectroscopy allows investigating molecular orientation by analyzing the vibration in a particular axis or plane. It has been observed that every molecule does not have spherical symmetry, therefore the interaction between the molecule and incident light changes in accordance with the polarization corresponding to the molecule orientation.

There are two type of polarization, perpendicular and horizontal polarization generally used. In order to generate these polarization, a half-wave plate and linear polarizer are used. The half-wave plate in optical path used to change the direction of polarization. After half wave plate, the laser is not completely polarized, or still remained a few polarizations through half wave plate, so one should cut those polarization by using polarizer. Polarizer lets only the light in one direction and cuts other directions. These polarized lights are parallel to the sample plane, so we can apply

this technique effectively to the one or two-dimensional material lying in the substrate. In addition, it allows us to know the molecular orientation by investigating the intensity ratio of perpendicular and horizontal polarization.

In general, there are two types of polarization, perpendicular and horizontal polarization used in optical experiments. These polarizations can be achieved with the help of a half-wave plate and a linear polarizer. The half-wave plate in the optical path changes the direction of polarization. The laser does not necessarily achieve the complete linear polarization, hence it is often required to cut the remained portion using a polarizer. Polarizer lets the light travel in only one direction and cuts other directions. These polarized lights are parallel to the sample plane when focused by an objective lens, so this technique can be applied effectively to the one or two-dimensional material lying in the substrate. In addition to that, investigation of the intensity ratio of perpendicular and horizontal polarization reveals the orientation of molecules. In order to investigate the orientation of a molecule with a three-dimensional structure, for example, pentacene molecule, it is essential to detect the vibration perpendicular to the substrate plane if they stand on the substrate. A Z-polarizer creates a polarized light in the direction of light propagation. The Z-Polarizer changes any linearly polarized light into radial or azimuthal polarized light as shown in Fig. 1-3. The direction of polarized light through the Z-polarizer differentiates the generation of radial or azimuthally polarized light. When the perpendicularly polarized light passes through the Z-polarizer, the light becomes radial polarized, and direction of polarization of this light would be in the direction perpendicular to the substrate plane when focused on the sample plane

using an objective lens. On the other hand, when the horizontally polarized light passes through Z-polarizer, the light is azimuthally polarized that can have direction parallel to substrate plane when focused on the sample plane using an objective lens. Thus, the ratio of Raman intensity under these two polarizations can be utilized in determining the orientation angle of a molecule. Thus, a three-dimensional orientation of molecules and crystals can be analyzed using the abovementioned two polarization techniques.

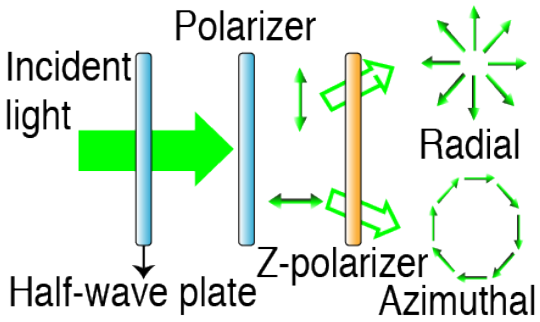


Fig. 1-3. Radial and azimuthal polarization of incident light

Polarization-dependent Raman spectroscopy is being applied to deepen the understanding of the material structure that could reveal the interesting properties of the material. The below section discusses some of the applications of polarization-dependent Raman spectroscopy.

1.3 Application of polarization dependent Raman spectroscopy

Polarization-dependent Raman spectroscopy has been used extensively in investigating properties of the crystal, such as local defect, crystal structure, and polymorphs. For instance, the study of Raman peak observed in Polarization-dependent Raman spectroscopy reveals various features of the material, which would have been a cumbersome task otherwise. The width of a Raman peak and the shift in the peak position can be utilized to study the crystallinity and the mechanical stress of a sample. Furthermore, several insights can be established with the assistance of the Raman image of the crystal, which can be attained by scanning the sample over laser focus, utilizing the advantage of polarization-dependent Raman spectroscopy. Several researches have been conducted in the past with an aim to study the semiconductor material by polarization-dependent Raman spectroscopy.[24,25] The work reported by R. Ossikovski et al., is one such research that revealed stress in strained silicon using polarization-dependent Raman spectroscopy.[26] The study of wide-gap semiconductor and organic semiconductor materials have gained much attention in the recent years.[27,28] The study of Liquid crystal is the other field that has gained the researcher's interest significantly.[29] The study of the distribution of the crystal structure with the polarization-dependent Raman spectroscopy is advantageous in investigating various organic semiconductor and the liquid crystal structure in detail. Moreover, the study of polarization-dependent Raman spectroscopy can also reveal the non-crystalline nature of the material, which is fundamental for investigating the low crystallinity samples.

The carbon nanotube is a unique one-dimensional material that has very high polarization sensitivity.[30] The performance of the carbon nanotube-based devices lies in the orientation of the molecular structure, which can be investigated in detail using the concept of polarization-dependent Raman spectroscopy. In a carbon nanotube polarizer[31], where Carbon nanotubes are unidirectional-aligned in a polymer, the higher polarization contrast of light transmitting the polarizer can be achieved by aligning the carbon nanotubes. Polarization-dependent Raman spectroscopy can be advantageous in understanding the quality of the aligned carbon nanotubes. Carbon nanotubes have several astonishing properties like extremely high electron mobility and signal-to-weight ratio.[32,33] These properties are attracting the researchers' attention to exploring the fascinating world of carbon nanotubes, which can be utilized in the development of electronic devices. The polarization-dependent Raman spectroscopy is a promising technique that can be utilized in the development of electronic devices based on carbon nanotubes.

In the field of polymer science, it is sometimes required to investigate the molecular orientation.[34,35] Researches in this field often employ the polarization-dependent Raman spectroscopy to investigate the molecular orientation. In general, polymers where elastic deformation is constrained, stress can alter the molecular orientation. Consequently, the molecular orientation is used as an indicator to analyze the stress characteristics of the polymer.

In the field of biological science, imaging the living cells is essential to explore the functionality of those cells.[36] The constituted molecules in the living cells are

usually oriented in a particular pattern. Therefore, Polarization-dependent Raman spectroscopy has been an essential tool to study the orientation of such molecules within the cells.

The application of polarization-dependent Raman spectroscopy has been extended to the field of organic semiconducting materials, where it is being used to measure its orientation. The research of Mino et al., had characterized the orientation of the pentacene molecule using polarization-dependent spectroscopy.[37] The presence of impurity and nature of the substrate used in the fabrication procedure influences the alignment of organic semiconducting molecules, which can affect electronic device performances. Hence, studying alignments in real electronic devices would be necessary.

Summary

I have discussed about the fundamental of the Raman scattering and the polarization-dependent Raman spectroscopy that provide information about the molecular structure and orientation. The polarization-dependent Raman spectroscopy has been utilized in the field of crystallography, polymer science, and biological science and is very useful, especially for the investigation of organic molecules.

References:

1. K. Nakamoto, Infrared and Raman Spectra of Inorganic and Coordination Compounds 5th ed., John Wiley & Sons: New York (1997).

2. R. A. Nyquist, Kagel, et al., M. Academic Press: New York (1996).
3. Introductory Raman Spectroscopy; Academic Press: New York, (1995).
4. B. Schrader, D. Bougeard, Eds.; John Wiley & Sons: New York, (1995).
5. J. Twardowski, P. Anzenbacher, and Ellis Horwood, Ltd., Chichester, U.K., (1995).
6. J. J. Laserna, Ed.; Wiley: Chichester, U.K., (1996).
7. G. Turrell, and J. Corset, Raman Microscopy. J., Eds.; Academic Press: New York, (1996).
8. G. Davidson, Spectrosc. Prop. Inorg. Organomet. Compd. 29, 248 (1996).
9. S. K. Saikin, et al., Phys. Chem. Chem. Phys., 11, 9401 (2009).
10. X. Zhang, N. C. Shah, and R. P. Van Duyne, Vib. Spectrosc., 42, 2 (2006).
11. A. Smekal, Naturwissenschaften, 11, 873 (1923).
12. C. V. Raman, K. S. Krishnan, Nature, 121, 501 (1928).
13. M. K. Anne, Annu. Rev. Phys. Chem. 61, 41 (2010).
14. D. Benjamin, C. Dana, S. Michael, and P. Jürgen, Introduction to the Fundamentals of Raman Spectroscopy.
15. L. L. Andrew et al., Anal. Chem. 70, 341-361 (1998).
16. R. D. Ziegler, Raman Spectroscopy (2006).
17. J. D. Trevor, Chemical Physics Letters 459, 180 (2008).
18. A. B. Myers, Ed. J. Raman Spectrosc. 27(8) (1996).
19. H. G. M. Edwards, Ed. J. Raman Spectrosc. 26, 911 (1995).
20. L. D. iegler, A. B. Myers, Eds. J. Raman Spectrosc. 1995, 26, 493.

21. Skoog, Holler and Nieman, Principles of Instrumental Analysis, fifth edition.
22. R. M. Martin, L. M. Falicov, Light Scattering in Solids I (Springer Series in Topics in Applied Physics vol 8), ed. M. Cardona (Berlin: Springer) chapter 3, 70 (1983).
23. E, Smith, and G. Dent, Modern Raman Spectroscopy: A Practical Approach, John Wiley & Sons, Ltd. (2005).
24. C. T. Chien, M. C. Wu, C. W. Chen, H. H. Yang, J. J. Wu, W. F. Su, C. S. Lin, and Y. F. Chen, Appl. Phys. Lett. 92, 223102 (2008).
25. K. F. McCarty, J. Z. Liu, R. N. Shelton, and H. B. Radausky, Phys. Rev. B, 41, 8792 (1990).
26. R. Ossikovshi, Q. Nguyen, G. Picardi, and J. J. Schreiber, Appl. Phs., 103, 0935259 (2008).
27. C. Hasio, L. Tu, T. Chi, M. Chen, T. Young, C. Chia, and Y. Chang, Appl. Phys. Lett., 90. 043102 (2007).
28. N. Muraki, and M. Yoshikawa, Chem. Phys. Lett., 481, 103-106 (2009).
29. M. S. Park, B. J. Yoon, J. O. Park, V. Prasad, S. Kumar, and M. Srinivasarao, Phys. Rev. Lett., 105, 027801 (2010).
30. G. S. Duesberg, I. Loa, M. Burghard, K. Syassen, and S. Roth, Phys. Rev. Lett., 85, 5436-5439 (2000).
31. S. Shoji, H. Suzuki, R. P. Zaccaria, Z. Sekkat, and S. Kawata, Phys. Rev. B, 77, 153407 (2008).

32. E.S. Snow, P.M. Campbell, M. G. Ancona and J.P Novak, Appl. Phy. Lett., 86, 033105 (2005).
33. I. Kang, Y. Y. Heung, J. H. Kim, J. W. Lec, R. Gollapudi, S. Subramaniam, S. Narasimhadevara, D. Hurd, G. R. Kirikera, V. Shanov, M. J. Schulz, D. Shi, J. Boerio, S. Mall and M. R. Wren, Composite: Part B, 37. 382 (2006).
34. C. Sourisseau, Chem. Rev., 104, 3851-3891 (2004).
35. A. S. Nielsen, and R. Pyrz, Composite Science and Technology, 62, 2219-2227 (2002).
36. T. S. Spiro and T. C. Strekas, Peoc. Nat. Acad. Sci., 69, 2622 (1972).
37. T. Mino, Y. Saito, H. Yoshida, S. Kawata, and P. Verma, J. Raman Spectrosc. 43, 2029–2034 (2012).

Chapter 2. Raman spectrum calculation by density functional theory (DFT)

One of the fundamental ways to identify and understand the internal architecture of molecules is to characterize its chemical bonding and intermolecular bonds. Raman spectrum provides this insight by giving information about the vibrations associated with such bonds. Detailed analysis of Raman peaks can be done using density functional theory (DFT). DFT calculation for a many electron system is based on an approach in which electronic structure is expressed as the total energy of ground state which is considered as a "function" which is a function of a function of an electron density.[1,2] This chapter describes the calculation of the electronic structure using DFT, and explains the calculation of normal vibrational frequency and Raman spectra.

2.1 Electronic structure calculation by DFT

The Physical and chemical properties of materials are very much dependent on their electronic structures. Calculation of electronic structure using DFT requires solving the Kohn-Sham equation which is an eigenvalue equation expressed as[3-5]:

$$\mathrm{F}\phi_i = \epsilon_i \phi_i \tag{2.1}$$

Where ϕ_i is the i-th molecules orbital, ϵ_i is the orbital energy, and F is the Fock operator given as follows:[1]

$$\mathrm{F} = \mathcal{H} + 2\sum_{j}^{n} \mathcal{J}_j + V_{XC} \tag{2.2}$$

The Fock operator operates to the eigenvalues of molecular orbitals resulting in the molecules orbital energy. $\mathcal{H}$ is the Hamiltonian operator related to one electron and expresses the Coulomb interaction between the core and electrons, and $\mathcal{J}_j$ is the Coulomb operator providing the coulomb interaction between two electrons. V_{XC} is the exchange interaction and electron correlation potential functional in order to account for the other interactions such as the exchange interaction and the electron correlation. Using equation (2.1) and (2.2), we can obtain the orbital energy as below.[1]

$$\epsilon_i = \int d^3\, r_1 \phi_i^* \mathrm{F} \phi_i(r_1) = h_i + 2\sum_{j}^{n} J_{ij} + \int d^3\, r_1 \rho_i(r_1) V_{XC} \tag{2.3}$$

where h_i and J_{ij} are given using below equations. [1]

$$h_i = \int d^3\, r_1 \phi_i^*(r_1)\ h\phi_i\,(r_1\,) \tag{2.4}$$

$$J_{ij} = \int d^3\, r_1 d^3 r_2 \phi_i^*(r_1)\phi_j^*(r_2)\frac{1}{r12}\ \phi_i\,(r_1\,)\phi_i(r_2) \tag{2.5}$$

h_i consists of kinetic energy of one electron and potential energy of the coulomb interaction between core and electron in the i-th orbital and J_{ij} consists of the potential energy of the coulomb interactions between two electrons.

The total electron energy is defined as the sum of the orbital energies, ϵ_i, for all electron states which is a total sum of Eq. (2.3) and is given by below equation.[1]

$$E = \sum_{i}^{n}(h_i + 2\sum_{j}^{n} J_{ij}) + E_{XC} \tag{2.6}$$

$$V_{XC} = \frac{\delta E_{XC}}{\delta \rho} \tag{2.7}$$

Where E_{XC} denotes the exchange –correlation energy functional and V_{XC} denotes the exchange-correlation potential functional which is expressed as the first derivative of the exchange-correlation energy functional with respect to an electron density.

Taking LCAO-MO approximate, the molecular orbitals, ϕ_i, can be express as following equation.[1]

$$\phi_i = \sum_{p}^{n_{AO}} C_{pi}\, X_p \tag{2.8}$$

where $\{X_p\}$ means the atomic orbital sets, n_{AO} is the number of atomic orbital and the expanding coefficient C_{pi} is the called molecular orbital coefficient. Atomic orbitals are Slater- type function, such as Aexp(-ξr), and Kohn-Sham equation is solved by the molecular orbital, ϕ_i shown in Eq. (2.8).

Gaussian-type function, such as Bexp ($-\alpha r^2$), is preferred over Slater- type function for simplicity of the calculation with computers.[6]

6-311G (d) is one of the most often used basis function, among various available options, as the obtained result has enough reliability for a practical use. However, a more accurate function 6-311G(d,p) is used in this study where a diffused function is added to 6-311G(d) for more accurate imitation of a real electric orbital. The symbol "p" means that this function takes in to account the influence of p-orbitals in the hydrogen atoms of a model system.

Diffused function is introduced for the simulation of loan pairs and bond orbitals in order to take in to account the effect of other orbitals not taking part in the chemical bonding but still has non-negligible effect.

6-311G(d) basis function is mainly applicable for only for a system with small molecular weight, however, LANL2DZ basis function is applied to a system with transition metal.[7] Hence, LANL2DZ is included in the effective core potential basis sets for the computation of DFT where core electrons are approximated by a potential because they do not influence chemical bonds or reactions. The computation result depends on the chosen basis functions and parameters in Eq. (2.2). The 1st and 2nd terms in the right side of Eq. (2.2) are the Hamiltonian operator and the Coulomb operator, representatively, which are known quantities, whereas, the exchange correlation potential functional, V_{XC}, is an unknown quantity and taken as inputs in the study.[8]

Once the basis function and potential functional are chosen, it is possible to calculate the Kohn-Sham equation, Eq. (2.1), following the steps below –

Step 1: Set the initial condition about the molecular system information (i.e core coordinator, core charges, and electron number) and the reference orbital.

Step 2: Calculate the Fock operator using the reference molecular orbital and eq. (2.2).

Step 3: Solve eq. (2.1) by inserting the calculated Fock operators into eq. (2.1.)

Step 4: Compare obtained molecular orbital and total electron energy to the former values

Step 5: Calculate exchange correlation energy using obtained molecular orbital and the total electron energy using eq. (2.6).

It is further required to set a threshold for the obtained solution as the solution is not uniquely determined using the method described above. Only by comparing to the set threshold it is possible to obtain molecules orbitals and total electron energies.

2.2 Calculation of molecular normal modes in Gaussian

Considering two atoms as point masses m and M. If the atoms are assumed to be connected by a spring with spring constant K, the displacement, x, and the reduced mass, μ, cab be defined as below.[1]

$$x = R - R_e\,, \qquad \mu = \frac{mM}{m+M} \tag{2.9}$$

Where, R is the as the distance between two cores and R_e is the balance distance between the two atomic cores.

The motion of this harmonic oscillator can be expressed as one particle motion as below differential equation.[1]

$$\mu \frac{d^2x(t)}{dt^2} = \ -kx(t) \tag{2.10}$$

A standard solution of the above equation is given by below.[1]

$$x(t) = Acos\sqrt{\frac{k}{\mu}}\ t \ + \ Asin\sqrt{\frac{k}{\mu}}\ t \tag{2.11}$$

where, A, B are arbitrary constants. Comparing this with the case of simple harmonics motion in the angle frequency of $\sqrt{\frac{k}{\mu}}$, we get the frequency as below.[1]

$$\nu = \frac{1}{2\Pi}\sqrt{\frac{k}{\mu}} \tag{2.12}$$

The potential energy in this model can be given as: $V(x)= kx^2/2$. Carrying out Tylor expansion of this potential energy, we obtained the below equation.[1]

$$V(x) = V(0) + \left(\frac{dV}{dx}\right)_{x=0} x + \frac{1}{2}\ \left(\frac{d^2V}{dx^2}\right)_{x=0} x^2 + \cdots \tag{2.13}$$

The displacement between the atoms is assumed to be small, which allows to neglect higher order terms in Eq. (2.13). At x=0, the two atoms are in equilibrium in the terms of forces. Force is the first derivative of potential energy, hence, at x=0,[1]

$$\left(\frac{dV}{dx}\right)_{x=0} = 0 \tag{2.14}$$

Substituting Eq. (2.14) into Eq. (2.13), and considering the potential energy at stable pointing as zero, we can obtain the formula for the potential energy as below.[1]

$$V(x) = \frac{1}{2} \left(\frac{d^2V}{dx^2}\right)_{x=0} x^2 \tag{2.15}$$

This suggests that the spring constant corresponds to the second derivatives of the potential energy (comparing with $V(x)= kx^2/2$). Once the derivative of the potential energy is calculated, it is possible to calculate the spring constant and the frequencies of the normal modes.

2.3 Calculation of Raman scattering in Gaussian

It is possible to compute Raman activities of sample molecules by calculating the derivatives of the polarizabilities with respect to the atomic coordinates. Polarizabilities can be determined by the perturbation calculation of the molecular energy towards the virtual electronic fields.

Assuming that the molecule under investigation has the characteristics vibrational mode, i, the differential Raman scattering cross section can be written as below.[1]

$$\frac{d\sigma_i}{d\Omega} = \frac{(2\Pi\nu_s)^4}{c^4} \left[e_s \frac{\partial \propto}{\partial Q_i} e_L\right]^2 \quad \frac{h(n_i^b + 1)}{8\Pi^2 \nu_i} \tag{2.16}$$

$$n_i^b \;=\; [\exp\left(\frac{h\nu_i}{kT}\right) - 1]^{-1} \tag{2.17}$$

Here, ν_s is the frequency of scattering lights, e_s, e_L are the unit vector toward the direction of the electronics fields of scattering and incident lights, respectively. $\propto$ denotes the polarizability tensor and n_i^b is the term related to the Bose-Einstein statistics, c is the velocity of light, and h is the Plank constant. Q_i represents a normal coordinate.

Assuming that the directions of incident light, and polarizabilities, and scattering lights can be regarded as parallel to the each, Eq. (2.16) can be written as:[1]

$$\frac{d\sigma_i}{d\Omega} = \frac{(2\Pi\nu_s)^4}{c^4} \frac{h(n_i^b + 1)}{8\Pi^2 \nu_i} \frac{S_i}{45} \tag{2.18}$$

where S_i is Raman activity whose unit is Å/amu. We can expand S_i using the nine components of the polarizabilities tensor as below.[1]

$$S_i = g_i \left[45\left(\frac{\partial \propto}{\partial Q_i}\right)^2 + 7\left(\frac{\partial \beta}{\partial Q_i}\right)^2\right] = 45\ \propto'^2 + \ 7\beta'^2 \qquad (2.19)$$

$$\propto' = \frac{1}{3}\ (\propto''_{xx} + \ \propto''_{yy} + \propto''_{zz}) \qquad (2.20)$$

$$\beta' = \frac{1}{2}\ [(\propto''_{xx} - \ \propto''_{yy})^2 + \ (\propto''_{yy} - \ \propto''_{zz})^2 + \ (\propto''_{zz} - \ \propto''_{xx})^2 + \ 6\ (\propto''_{xy}{}^2 + \propto''_{yz}{}^2 + \propto''_{zx}{}^2)] \qquad (2.21)$$

In Eq. (2.20), $\propto''_{xx}$ means the derivatives of the xx component in the tensor with the respect to the normal coordinate, Q_i . g_i is degeneracy of the tensor. Raman activity of the molecule can be obtained by injecting the components of a polarizability tensor into equations (2.19) – (2.21), we can obtain a Raman activity.

Further, we need to calculate the components of a polarizability tensor. The perturbation of the energy towards the external electronic fields is essential for this calculation. External electronic field can be considered as the constant at the molecular scale and is defined by below.[1]

$$F\ =\ -\ \Delta\ \phi \qquad (2.22)$$

The condition, such as, x=0 and F=0 as in equations (2.14) and (2.22), are necessary to calculate Raman activity. Due to this reason, the calculations are based on the fact that input molecules should be in the state of balance that reflects the optimized

structure of the molecule. The optimized structure provides the reliable results with the different basis functions used in the calculation.

The Raman activity of a molecule indicates the possibility of the occurrence of Raman scattering that results in the Raman intensity of a specific vibrational mode. The result obtained from Gaussian cannot provide a real Raman intensity of the vibrational mode as it does count the effect of incident laser and a possible heat in the measurement system. Therefore, it is not feasible to compare the experiment Raman intensity with the calculated Raman intensity. In order to compare the result in the calculation with that in the experiments, the following formula was suggested, which give a relationship between Raman intensity with the absolute intensity.[1]

$$I^{Raman} = \frac{C(\nu_i - \nu_s)^4 S_i}{\nu_i \, n_i^b} \quad [a.u.] \qquad (2.23)$$

Where C is the experimental constant, and the value of this constant was adopted as 10^{-12}.[6] If we compare the DFT calculated result with the experimental ones, the key is whether we use Raman activity or absolute Raman intensity defined in Eq. (2.23) as the simulation result. In the case of a comparison of the Raman peak position, the results are reliable and help in getting information about the vibrational properties of the molecules at a specific vibrational mode.

Summary

In this chapter, I have discussed about the calculation of the electronic structure using the density functional theory (DFT). Then, the calculation of the normal vibrational frequency and Raman spectra using DFT are also explained in detail.

References:

1. T. Tsuneda, Density Functional theory in quantum method, Kodansha (2012).
2. M. J. Frisch, Gausian 09, Revision C.01 (2009).
3. J. A. Pople, D. A. Beveride, Approximate Molecular Orbital Theory, McGraw Hill Book Comapany (1970).
4. M. Born, and J. R. Oppenheimer, Ann. Physik, 84, 457 (1927).
5. N. S. Szabo, Ostlund, Modern Quantum Chemistry: Introduction to Advance Electronic Structure Theory, McGraw Hill: New York (1989).
6. F. Jensen, Introduction to quantum chemistry, John wiley & sons (2006).
7. D. Porezag, and M. Pederson, Phys. Rev. B. 54, 7830-7836 (2010).
8. M. Alecu, J. Zheng, J. Zhao, and D. G. J. Truhlar, Chem. Theory Comput. 6, 2872-2887 (2010).

Chapter 3. Organic field effect transistor (OFET) devices

The scope of this study entails the investigation of Raman spectroscopy for transistor devices based on the organic molecule. This chapter incorporates the introduction of organic field-effect transistor devices and its output characteristics with their applications.

3.1 Introduction of OFET devices

Organic field-effect transistor has vast applications in today's world. It is often used in displays, organic light-emitting diodes, integrated circuits (ICs), radio frequency identification tags (RFIDs) etc. It is considered an essential tool to explore the charge transport characteristics of organic semiconductors as well. Charge carrier mobility, which is the measure of how fast the charge carriers move in a material, is fundamental to conceptualize the function of OFETs. This reflects the velocity at which charge carrier is flowing through the OFET channel in the presence of an electrical field. The strength of charge carrier mobility is fundamental to the decision on the applicability of the material to be used in semiconductors, eventually limiting the range of applications. Additionally, it also influences the parameters operation stability on/off ratios along with turn-on voltage.

The research on OFETs has witnessed significant progress over the last few decades in order to develop suitable material which has extended its application to many fields. The electrochemically polymerized polythiophene was used to develop the first

organic transistor in 1986.[1] This device had the hole mobility of about 10^{-5} cm^2/Vs, which was significantly lower than the benchmark amorphous-Silicon FETs. Later in 1994, Garnier et al. achieved a carrier mobility of 0.01 cm^2/Vs in an organic transitor.[2] Compared to amorphous-Si transistors, this mobility magnitude was only an order of magnitude lower. This allowed then to successfully develop a printing electronics with the help of screen printing of the source, drain, and gate electrodes used in the transistor. Further advancement in the research field led to the development of a small molecule vacuum evaporated organic semiconductor named *Pantacene* which exhibited mobility higher than 1 cm^2/Vs.[3] After a couple of years Bao et al. revealed to the scientific community for the first time that high carrier mobility can be attained with a conjugated polymers using regioregular (poly3-heaxylthiophene).[4] They further continued to develop the all- printed plastic transistors with a successful attempt in 1997.[5] The OFETs have been used extensively in the OLED display. At first, OLED display was developed with a single-pixel with an OFET switching i.e., on/off state of an OLED pixel.[6,7] Bell Labs and E-Ink further advanced had attributed to the evolution of flexible electronic paper display where radio frequency tags were reported.[8,9] The high mobility magnitude had firmed the importance of OFETs in the development of several electronic devices.

3.2 Output characteristics of OFET

This section introduces the principles of OFET operation and procedures to realize the electrical characteristics of OFETs. It is well known that an OFET has three terminals comprises of electrodes, a dielectric layer and an organic semiconducting layer, as presented in Fig. 3-1. The first terminal is the organic semiconductor film, which facilitates a pathway for charge transport. This layer is deposited through vapor or solution processes on the dielectric layer. The dielectric layer acts as a second terminal. Applied gate field near the interface of semiconductor/dielectric capacitively induces charges in the semiconducting layer. Non-conjugated polymers, e.g., polyvinyl phenol (PVP), polystyrene (PS), divinyl tetramethyl siloxane-bis(benzocyclobutene) (BCB) or Inorganic insulators, e.g., SiO_2 and Al_2O_3, in addition to a cyclic transparent optical polymer (Cytop) usually constitutes the dielectric material. The third terminal is the gate electrode. This can be made of a metal or a conducting polymer. Nature of charge carriers is illustrated by the polarity of gate bias. The heavily-doped Si wafer is typically a gate/insulator substrate which is covered with a thick layer (~100–300 nm) of SiO_2. It is being used for the evaluation of organic semiconductors as it is readily commercially available. The voltage gradient is generated with the help of drain and source electrodes. This is the primary reason for the flow of current in the channel. Usually, the source and drain electrodes are fabricated with a shadow mask via a thermal vapor deposition method. Channel length, L, is defined by the distance between drain and source electrodes, whereas, the width of drain and source electrodes are termed as the channel width, W.

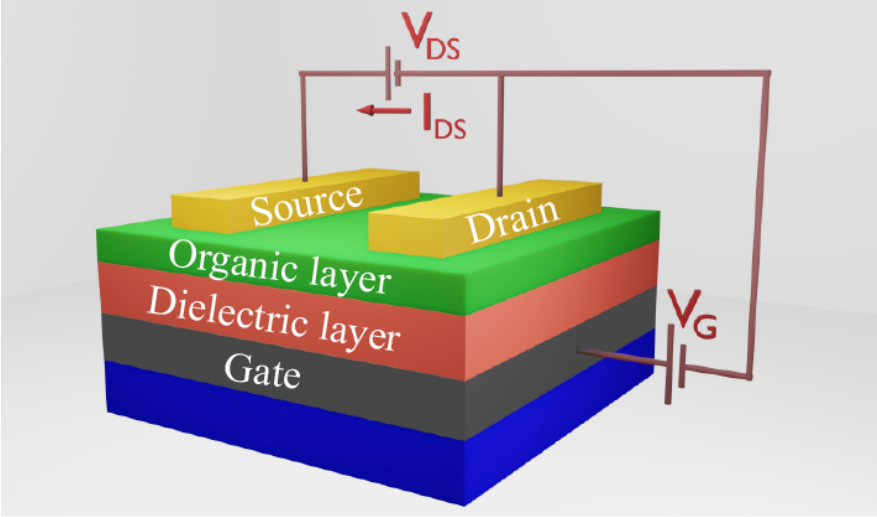


Figure 3-1. A schematic representation of OFET device structure

The applied gate voltage (V_G) and drain-source voltage (V_{DS}) determines the amplitude of the drain-source current (I_{DS}). The characteristics between current and voltage are the fundamental entity, which is used to deduce the OFET trait. In general, the OFETs are assessed by two sweeping approaches, commonly represented as the output curve, and the transfer curve. The output curve approach can be implemented by varying V_{DS} at different set values of V_G. The flow of current due to the voltage generated depends on V_{DS}. Alternatively, when $V_G >> V_{DS}$, the current flow is directly proportional to V_{DS}. The range of voltage operation follows linear characteristics and often regarded as a linear regime. Another notable characteristic referred to as a saturation regime is the voltage range ($V_G - V_{TH} \leq V_{DS}$) when the current flow in a field-effect transistor doesn't depend on V_{DS} and gets saturated due to the pinch-off effect.

The second approach is the transfer characteristics elucidates the relation between I_{DS} vs. V_G at constant V_{DS}. The transfer characteristic is being used to determine various parameters including the mobility (μ). As explained above, Mobility is a parameter which assesses the velocity of charge carriers through the layer present in the semiconductor layer in an electrical field. The mobility parameter can be obtained from either the linear regime or saturation regime.

The expression for the drain current in the linear regime ($V_{DS} << V_G$), can be presented as shown below in Eq. 3.1:[10]

$$I_{DS} = \frac{W}{L} \mu_{lin} C_i (V_G - V_{TS}) V_{DS} \quad (3.1)$$

where C_i = capacitance of the gate dielectric per unit area,

W = Width of channel

L = Length of channel

The mobility in the linear regime, μ_{lin}, can be deduced from the slope of the linear fit of I_{DS} versus V_G.

The expression for the drain current in the saturated regime ($V_{DS} \geq V_G$), can be presented as shown below in Eq. 3.2:[10]

$$I_{DS} = \frac{W}{2L} \mu_{Sat} C_i (V_G - V_{TS})^2 \quad (3.2)$$

The value of the mobility in the saturation regime, μ_{Sat} can be directly deduced from the slope of the linear fit of $I_{DS}^{1/2}$ versus V_G.

It is worthwhile to note that in general, the mobility in the saturation regime is higher than those in the linear regime due to the fact that more charge traps being filled.

3.3 Application of OFET devices

Nature and associated properties OFET devices leads to various potential applications. Some of the devices which incorporate OFETs are explained below.

Displays: Development of large-area electronic displays are one of the areas where OFETs are extensively used. Development of active-matrix liquid crystal display (AMLCD) backplane architectures has been majorly possible due to Amorphous silicon (a-Si) FETs as the low process temperature facilitates low cost fabrication on large glass substrates with the additional advantage of satisfactory performance for LCD field driving. OFETs are extremely suitable for such backplane applications. One of the advantages of OFETs is that it shares many of the properties of a-Si LCDs but with a better thermal budget. The reduction in thermal budget facilitates the economical fabrication of plastic sheets, metal foils and glass etc. Mechanically flexible field-driven displays using OFETs on plastics and other substrates are depicted by many researcher groups in addition to a flexible polymer-dispersed LCD.

Mechanical sensors: The application of OFET is tremendously wide due to its large size and mechanical flexibility. In addition to that, it is advantageous in switching

actions and amplification of mechanical actuation. The work of Someya *et al*. reported the application of OFETs in a mechanical sensor for large- scale application for the first time. Backplane of the OFET was laminated with a flexible conductor with loaded elastomer. The resistance of the elastomer varied in accordance with the pressure applied.[11] It has been observed that variable-resistor based flow of current and switching operation through the transistor matrix can create a force map so as to develop a flexible sensor skin.



Figure 3-2. A very thin and light stretchable electronic device on skin. This image is taken from the article published online on the website.[12]

Imagers: Imaging sensing application also utilizes the benefit of large and flexible backplanes property along with the mechanical flexibility characteristics of OFETs. Organic semiconductors coupled with a single transistor per cell OFET and a photoconductor material such as titanylpthalocyaninie or an organic photodiode can be used for the purpose of image sensing. The architecture facilitates the development of fully additive photodetector elements on substrates like plastic sheets, non-planar surfaces or injection-molded objects.

RFID and logic: OFETs exhibits potential benefits in the development of logic elements and their different variants which opens up a lot of applications such as RFID for access. It has been believed that economics in line with paper printing can be achieved for the development of RFID and logic elements subjected to the condition that other supporting parts like tag antenna, transistors and various passive elements are produced using continuous printing processes simultaneously.

Summary

Organic electronics have gained enormous attention in the recent years due to their wide-range applications owing to its advantage in the development of flexible, printable, and large-area low-cost devices. This chapter covers the fundamentals, output characteristics, and application of OFET technology.

References

1. A. Tsumura, H. Koezuka, and T. Ando, Appl. Phys. Lett., 49, 1210 (1986).

2. F. Garnier, R. Hajlaoui, A. Yassar, and P. Srivastava, Science, 265, 1684 (1994).

3. S. F. Nelson, Y.-Y. Lin, D. J. Gundlach, and T. N. Jackson, Appl. Phys. Lett., 72, 1854 (1998).

4. Z. Bao, A. Dodabalapur, and A. J. Lovinger, Appl. Phys. Lett., 69, 4108 (1996).

5. Z. Bao, Y. Feng, A. Dodabalapur, V. R. Raju, and A. J. Lovinger, Chem. Mater., 9, 1299 (1997).

6. B. Crone, A. Dodabalapur, Y.Y. Lin, R. W. Filas, Z. Bao, A. LaDuca, R. Sarpeshkar, H. E. Katz, and W. Li, Nature, 403, 521 (2000).

7. H. Sirringhaus, N. Tessler, and R. H. Friend Science, 280, 1741 (1998).

8. A. Dodabalapur, Z. Bao, A. Makhija, J. G. Laquindanum, V. R. Raju, Y. Feng, H. E. Katz, and J. Rogers, Appl. Phys. Lett., 73, 142 (1998).

9. J. A. Rogers, Z. Bao, K. Baldwin, A. Dodabalapur, B. Crone, V. R. Raju, V. Kuck, H. Katz, K. Amundson, J. Ewing, and P. Drzaic, Proc. Natl. Acad. Sci. USA, 98, 4835 (2001).

10. S. R. Marder, and J. L. Bredas, The WSPC Reference on Organic Electronics: Organic semiconductors (2016).

11. A. Miyamoto, S. Lee, N. Cooray, Nature Nanotechnology, 12, 907, (2017).

12. https://www.u-tokyo.ac.jp/focus/en/articles/a_00590.html.

Chapter 4. Molecular orientation analysis of pentacene in OFET device by polarization dependent Raman spectroscopy

In this chapter, I will first introduce the pentacene molecule, after which the fabrication method and the output characteristics of the fabricated transistor device will be discussed. Later on, I will discuss about the analysis of the molecular orientation of organic pentacene with respect to their inclination angle in fabricated transistor devices by studying it with polarization-based Raman spectroscopy technique.

4.1 Introduction of organic semiconductor molecule pentacene

Pentacene molecule ($C_{22}H_{14}$) is a polycyclic aromatic hydrocarbon with five fused benzene rings, as illustrated in Fig. 4-1. It occurs fifth in the aromatic series starting with benzene, naphthalene, anthracene, and tetracene and is a highly conjugated organic semiconductor compound. After absorption of visible or ultraviolet electromagnetic radiation, it releases excitons and its sensitivity towards oxidation is extremely high. Considering these facts, pentacene, which has purple in color and in powder form, slowly degrades upon exposure to light and air.

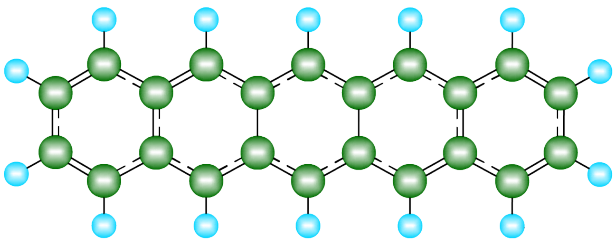


Figure 4-1. Structure of pentacene molecule. Blue and green spheres represent hydrogen and carbon atoms.

The pentacene molecules has been subject of extensive study viewing it as an important candidate for the electronics devices among the several available organic materials.[1,2] In terms of performance, pentacene was the first vacuum evaporated organic semiconducting molecule, which showed a mobility value larger than 1 cm^2/Vs. Various factors contributes to affect the performance of the transistor devices fabricated with pentacene molecules which includes the grain size, molecular orientation, and the presence of impurities.[3-8] The alignments of pentacene molecule significantly alters the flow charge flow by its carriers in the device. For example, if there is any alignment difference between neighboring molecules in the device, then it would result in degradation of the overlap of the π electrons between them. As a result, it would cause an interruption of the charge carrier flow in the device that has the capacity of affecting the device performance. Therefore, understanding molecular alignments of pentacene molecules and subsequently its effect on transistor device performance would be necessary for further improving their performance.

4.2 Fabrication method and electronic characteristics of the transistor device

Understanding the effect of molecular orientations of the pentacene molecules for device performance, two different types of samples were fabricated. One, kind of transistor device includes sublimated and others includes non-sublimated. Fabrication was done under otherwise similar conditions. The non-sublimated pentacene molecules contain some impurities, for example, aluminum, iron, 6,13-dihydropentacene, and

6,13- pentacenequinone. The impurity in non-sublimated molecules can be removed using the sublimation process to get a sublimated pentacene sample that contains almost no impurity.

I received pentacene based transistor devices from Prof. Sekitani's lab. The fabricated device is schematically displayed in Fig. 4-2. First, a 30-nanometer thin layer of Al was deposited on a cleaned glass substrate with vacuum deposition technique. This substrate was later dipped into 1 millimolar of citric acid ($C_6H_8O_7$) for the anodization where aluminum oxide (AlO_x) layer was grown over it. Further on, this substrate was kept in 3 millimolar of dodecylphosphonic acid ($C_{12}H_{27}O_3P$) at 30°C temperature for 12 hours, afterward it was cleaned and dried with isopropanol and a stream of nitrogen, respectively that generates the dodecylphosphonate self-assembled monolayer on the substrate. Afterwards, a 30-nanometer thin film of pentacene was vacuum deposited with a stable rate of 0.2 Å/s. Then, 50-nanometer thin layer of gold (Au) was deposited on the same substrate using a shadow mask that defines drain and source contacts of the transistor device. Finally, the complete device was put into vacuum at 100°C temperature for 1 hour for annealing. The width and length of the channel were 500 μm and 40 μm, respectively. Sublimated and non-sublimated pentacene molecules were used to fabricate two variant of transistor devices under otherwise similar fabrication conditions.

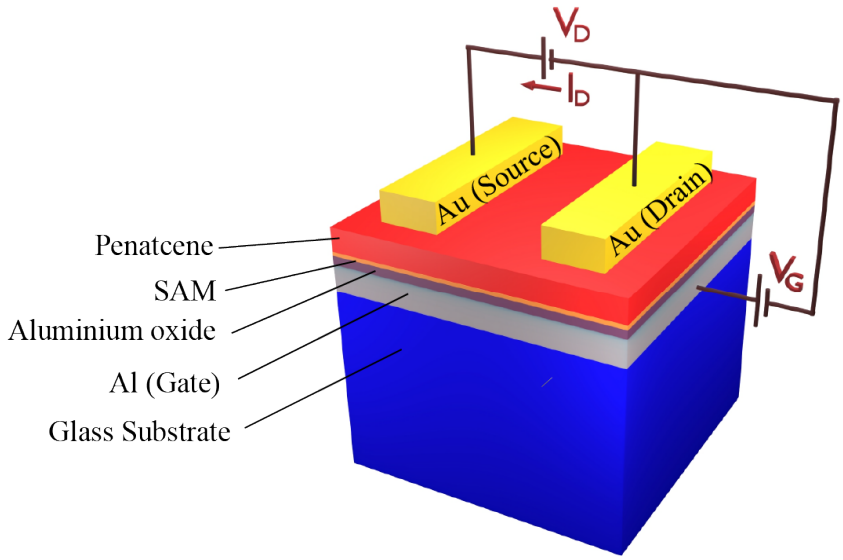


Figure 4-2 A schematic of the pentacene OFET device.

The electrical characteristics of the transistor device was measured by Prof. Sekitani's group. In order to measure, the device was connected with a drain-source voltage (V_D) and a gate-source voltage (V_G) as shown in Fig. 4-2. Device characterization for the sublimated and non-sublimated types were recorded and presented in Fig. 4-3 which shows the output characteristics and transfer curve. Measurement for the transfer curves were performed by changing the gate-source voltage from +0.5 to -3V with constant drain-source voltage at -3V, for sublimated and non-sublimated devices as seen in Figs. 4-3(a) and 4-3(b), respectively. The drain-source current of the device as a function of drain-source voltage i.e., output characteristics was measured by changing the gate-source voltage from +0.5V to -3V in steps of 0.5V. The output characteristics measured for the two types of devices namely, sublimated and the non-sublimated one are displayed in Figs. 4-3(c) and 4-3(d), respectively. The computed values of charge carrier mobilities for these fabricated

non-sublimated and the sublimated pentacene transistors devices were evaluated as 0.0352 $cm^2V^{-1}s^{-1}$ and 0.603 $cm^2V^{-1}s^{-1}$, respectively. From measurements, I concluded that the carrier mobility for the pentacene sublimated transistor was better than that of the non-sublimated pentacene transistor.

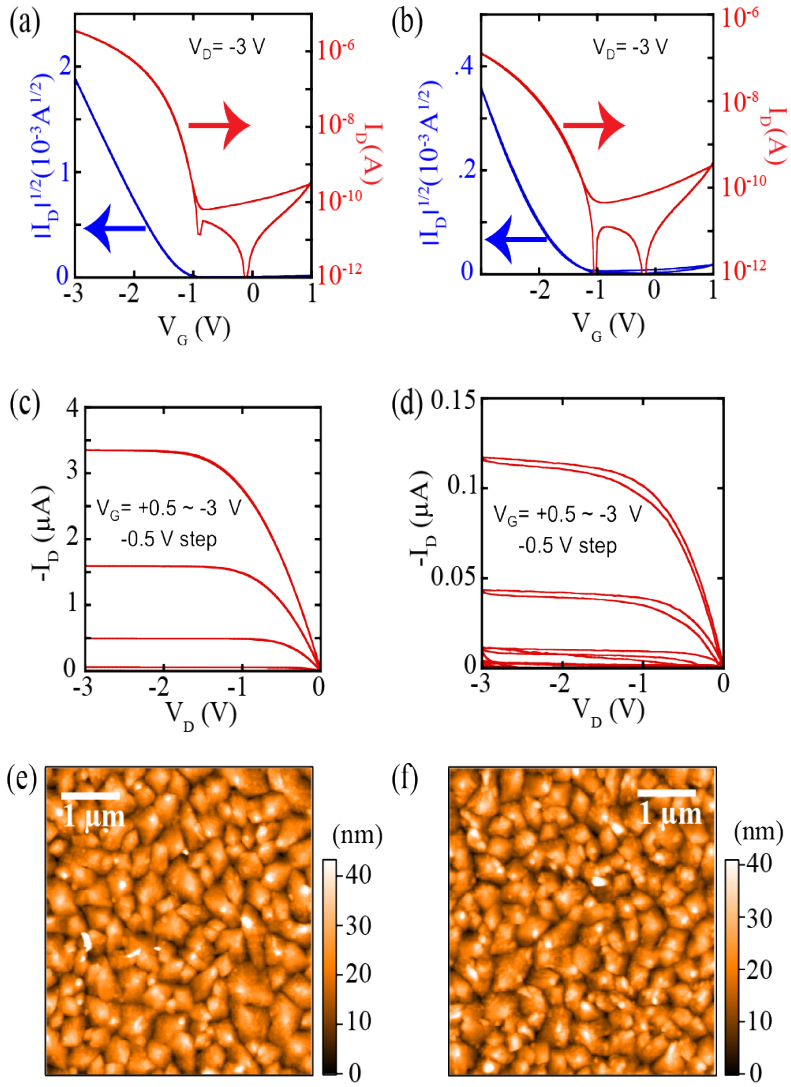


Figure 4-3. Transfer curves for the (**a**) sublimated and (**b**) non-sublimated pentacene transistor device, obtained output characteristics for the (**c**) sublimated and (**d**) non-sublimated devices, Atomic force microscopy images show morphologies of the (**e**) sublimated and (**f**) non-sublimated pentacene transistor devices.

4.3 Analysis of molecular orientation of pentacene in transistor devices

After measuring the higher mobility for the fabricated sublimated device, I turned my attention to understand the reasoning behind this high carrier mobility. I performed surface morphology study using atomic force microscopic (AFM) of both devices. AFM images presented in Figures 4.3(e) and 4.3(f) shows the morphology for the sublimated and non-sublimated devices. Previously, it has been reported that he surfaces morphology plays a major role in deciding the device performance.[9] However, in my case, I observed similar morphologies of pentacene in both fabricated devices with negligible changes in grain size of the pentacene molecules. Hence, morphologies of pentacene have little effect on the device performances as they were not noticeably affected by the sublimation process. These observations confirm that the AFM technique does not provide sufficient information for the devices. Therefore, to understand the cause of high mobility in the device, I performed Raman studies for both fabricated transistor devices.

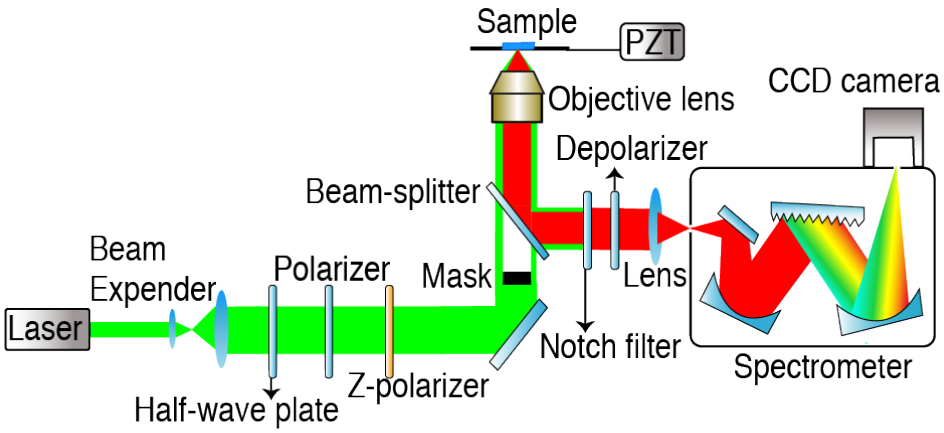


Figure 4-4. Experimental set-up for the Raman spectroscopy measurement.

Figure 4-4 illustrates the optical set-up utilized for the Raman studies in the backscattering configuration. A 532 nm laser was used for the excitation and was focused on the device plane using an objective lens of magnification 150× and a numerical aperture of 0.95. The laser beam passed through a series of optical equipment – first through a half-wave plate ($\lambda/2$ plate), then trough a linear polarizer, afterwards it passes through a z-polarizer, and a circular mask before it passes through the objective lens. Control of direction of the linearly polarized light was achieved using a half-wave plate and a linear polarizer. By introducing a z-polarizer and changing the linear polarization direction of the laser beam, from horizontal to vertical, I was able to generate azimuthal and radial polarization of the light, as displayed in Fig. 1-3 of chapter 1. Further, I used a small circular mask in the path way of light before the objective lens that blocks light with a small numerical aperture less than 0.8, and produces a strongly dominant normally polarized light at the device plane, as shown in Fig. 4-5 using a green arrow perpendicular to the device plane. As the Raman setup operates in a backscattering configuration, the scattered light from the device was collected using the same objective lens. Finally, the collected Raman scattered light was passed through a depolarized and dispersed with a spectrometer having a grating of 1800 grooves per mm and detected using a CCD camera. Rayleigh scattered light blocked by use of notch filter before the light goes into the spectrometer. As I mentioned, I utilized two sets of polarizations, radial and azimuthal polarization, in my experiment. After passing through an objective lens, the directions of radial and azimuthal polarizations become in the direction of perpendicular and parallel to the

device plane, respectively, as illustrated in Fig. 4-5. It is reported that the pentacene molecule grows nearly vertical direction on the AlO_x/SAM substrate.[11] Also, the pentacene molecule has a vibrational mode (B_{3g} mode) at 1596 cm^{-1}, which shows atomic displacements along the parallel direction of the long-molecular axis of pentacene. Thus, the direction of atomic displacements of this mode would be along the perpendicular direction to the device plane if molecular orientation of the pentacene is normal to the substrate. Hence, I expect minimum Raman intensity for this specific mode in an azimuthal polarization of incident excitation, whereas Raman intensity would be maximum in case of the radial polarization of incident excitation. On the other hand, this effect would be the opposite if pentacene molecules lie on the device plane, i.e., maximum for azimuthal polarization and minimum for polarization. Hence, the ratio of Raman intensities for these two sets of polarizations of incident light would shed light on the tilt angle if pentacene molecules are aligned at a specific angle with respect to the normal direction of the device plane.

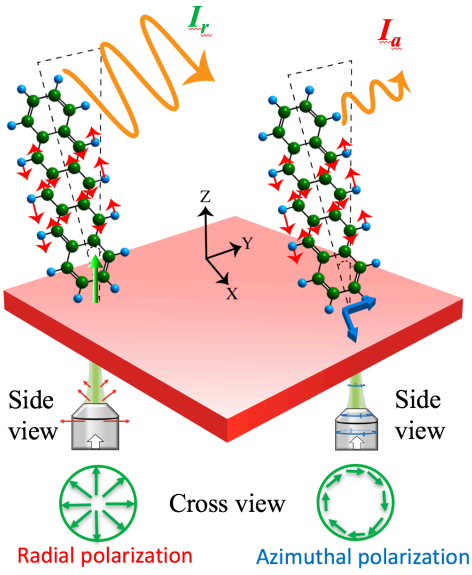


Figure 4-5. Molecular orientation analysis with radial and azimuthal polarization

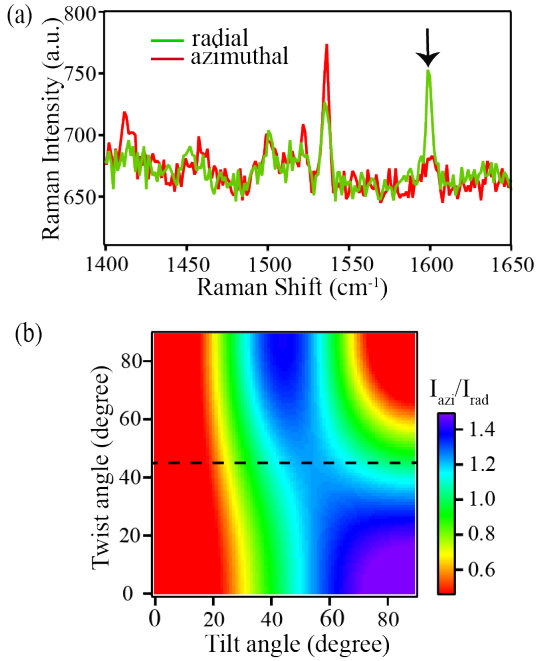


Figure 4-6. (**a**) Experimentally measured Raman spectra using 120 μW laser power and 3 second exposure. The green and red color Raman spectra obtained under radial and azimuthal polarizations of laser, respectively, at the same position. (**b**) dependence of the intensity ratio on twist and tilt angles using a theoretical calculation.

Raman signal of pentacene molecules was measured using radial and azimuthal polarization of laser beam, which is shown in Fig. 4-6(a). From the measurement it can be seen that the intensity of B_{3g} mode present at 1596 cm^{-1} drastically increases for the radial polarization of the laser in comparison to the azimuthal polarization. The other observed Raman modes also showed polarization dependence, but the Raman mode at 1596 cm-1 was more sensitive to the incident polarization of the laser beam. Therefore,

I selected this Raman mode for further investigations. The ratio of Raman intensities under azimuthal and radial polarizations of incident laser measured at the same position would help in determining the amount and nature of tilt angle of the organic pentacene molecules in transistor devices.[9]

To get insights into the nature and magnitude of the tilt angle, Raman intensity ratio to the orientation angle was converted by taking into account the possible parameters for the calculation. Calculated collection efficiencies for the incident polarization of the objective lens for two orthogonal polarization components, A and B, depends on the cone angle of the objective lens. The objective lens used in my experiment had a numerical aperture of 0.95, corresponding to a cone angle of 71.8 degree. The values obtained after calculation for A and B were 9.98 and 1.11, respectively. Pentacene molecule with standing geometry can show an inclination with respect to its vertical position, and simultaneously it can have twist along its molecular axis. Raman intensity is largely dependent on tilt angle as well as the molecular twist along the axis of pentacene molecules. Since I am talking about an intensity ratio, as observed from the color plot in Fig. 4-6(b), a single value of intensity ratio can be obtained by several different permutation and combination using the tilt angle and twist angle. Considering the fact that, molecular alignment of the pentacene molecules is nearly normal to the AlOx/SAM substrate, I can safely neglect the larger shift in the tilt angles as seen in the right-half of the color plot in Fig. 4-6(b). From this figure, it can be inferred that role of twist angle is not that dominant and intensity ratio largely dependent on the tilt angle of the molecule. As such we can fix this angle for

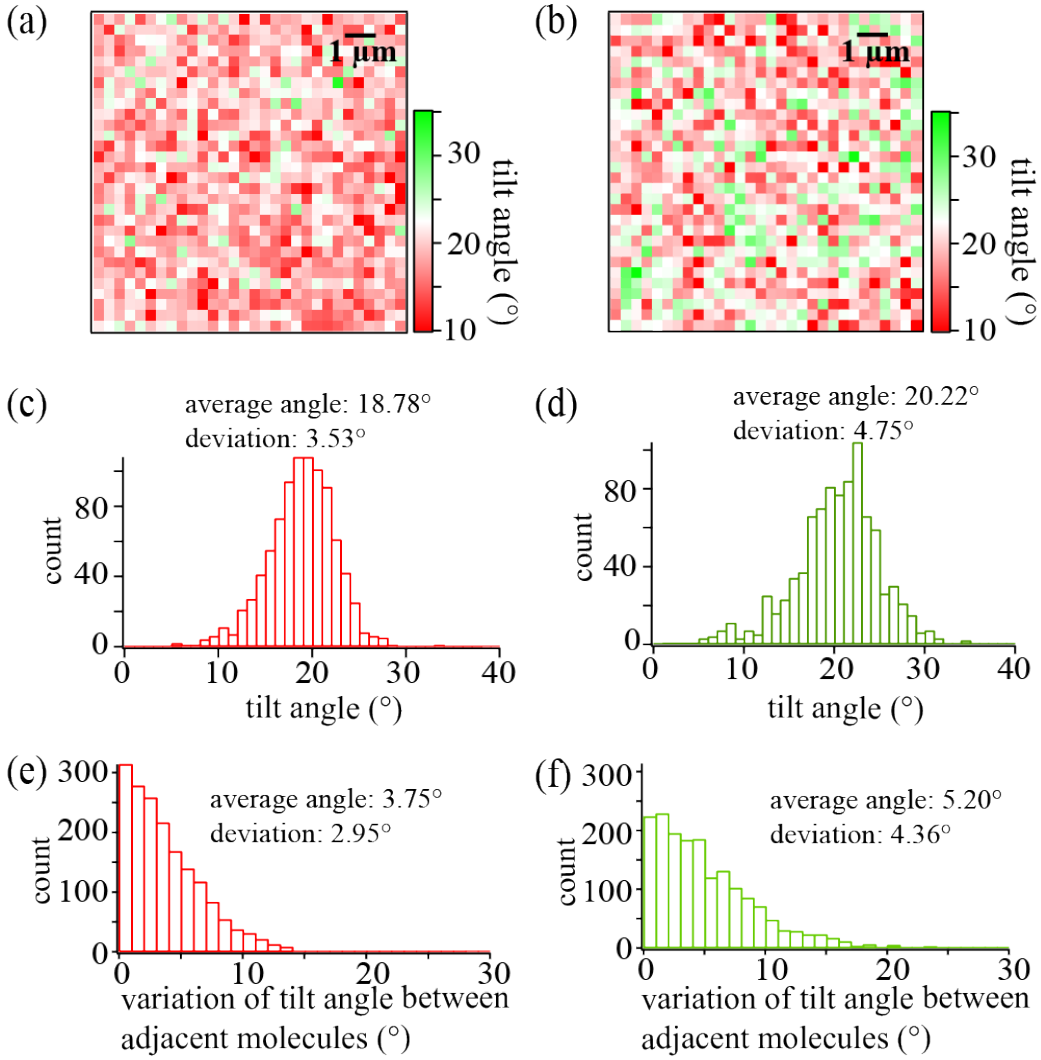


Figure 4-7. The orientation distribution of (**a**) sublimated and (**b**) non-sublimated pentacene transistor devices. Histograms show variation of tilt angle for (**c**) sublimated and (**d**) non-sublimated pentacene transistor devices, and histograms show the difference of tilt angle between neighboring positions for (**e**) sublimated and (**f**) non-sublimated pentacene transistor devices.

understanding the effect of molecular tilt angle. Twist angle was fixed to a value of 45 degree to find out the tilt angle as shown with the dashed line in Fig. 4-6(b). With this approach, Fig. 4-6(b) was taken as the reference point for the calculation of tilt angle for

the further measurements of intensity ratio and subsequently construct the Raman images of the tilt angle distribution in the two types of fabricated transistor devices. Such measurements were performed in 10×10 μm^2 areas of the device with 30×30 pixels.

Figures 4-7(a) to 4-7(b) display the spatial distribution of the molecular tilt for the two types of transistors fabricated with pentacene molecules together with its histogram for orientation image. For the sublimated device, the average tilt value of angle was calculated to be 18.78 ± 3.53 degree. But, the average value of the tilt angle was calculated to be 20.22 ± 4.75 degree for the non-sublimated device. From these measurements, I can deduce that the sublimated device shows a smaller tilt angle and its deviation is smaller as well. On the other hand, non-sublimated device shows a higher value. This cause the effective transportation of charge carriers from source to drain in the sublimated pentacene transistor device. The presence of several types of impurities such as aluminum, iron, 6,13-dihydropentacene, and 6,13- pentacenequinone, in non-sublimated pentacene can be a reason for its larger orientation angle. I suspect that while doing the vacuum deposition of pentacene layer, impurities molecules might have got deposited in between and, as after effect of this it may alter the tilt angle of pentacene molecules in the fabricated device, which in turn changes the carrier mobility. As observed earlier, sublimated device shows higher mobility than the non-sublimated one, however, the difference between the two types of devices for the average tilt angle was only 1.44 degree. This prompted me to further look into the cause of the significant

difference of carrier mobility of these two devices. To do that, I analyzed the variation of tilt orientation angle difference among all the neighboring measurement positions in the device utilizing the high spatial resolution. A reference point was chosen in such a way as to subtract the tilt angle at any particular spatial location from the tilt angle at its neighboring position. This spatial separation is in the order of few hundreds of nanometers in the device. Further one, based on these calculations I created a histogram map, which displays the variation of tilt angles among the neighboring pixels in devices as can be seen Fig. 4(e) and 4(f). From this measurement, indeed it is clear that for a large number of spatial positions the angle difference between the neighboring measurements are smaller for the sublimated device than the non-sublimated device. The average values obtained from these measurements for the sublimated device and non-sublimated device as 3.75°±2.95° and 5.20°±4.36°, respectively. Hence, I can confirm that the sublimated device shows smaller angle variation with a smaller standard deviation. So, the small angular difference with its neighboring positions enables effective transportation of carriers from one point to its nearest neighboring points. This effective transfer is in turn reflected as the higher carrier mobility of the sublimated device. Identical measurements were performed on the different parts of the device to confirm the claim of the effective transportation in wider areas of the device.

Figures 4-8 and 4-9 shows the spatial distribution of the angular inclination of the pentacene variations of angles with its neighboring positions which are separated by 100s of nm measured in five different regions of size 10 μm × 10 μm in both devices.

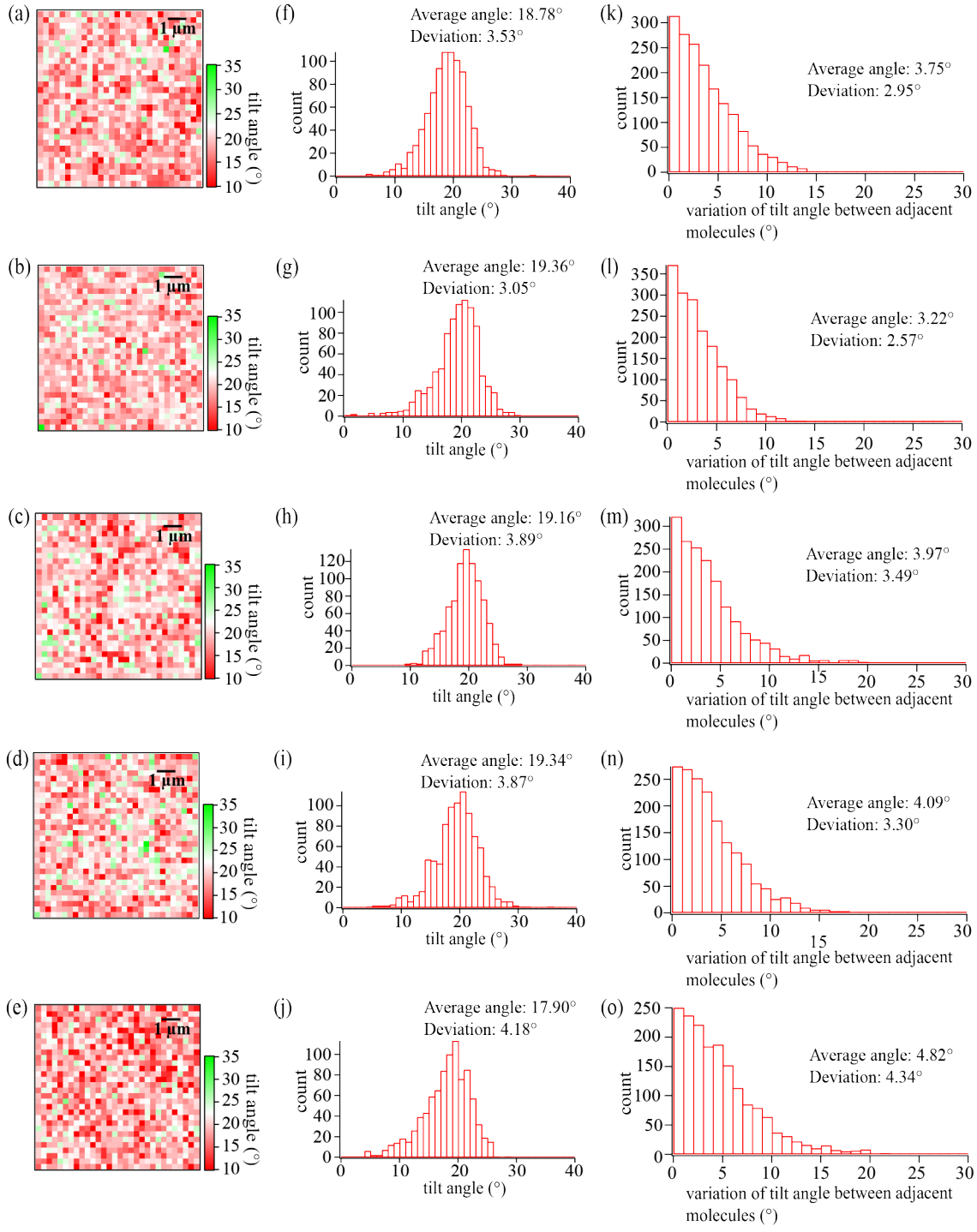


Figure 4-8. (**a**)-(**e**) show the molecular orientation distribution at five different regions of the sublimated pentacene transistor device. Histograms (**f**)-(**j**) show the corresponding tilt angle variation for the same five positions, and histograms (**k**)-(**o**) show the difference of the tilt angle between adjacent positions that is separated by few hundreds of nanometers in the transistor device.

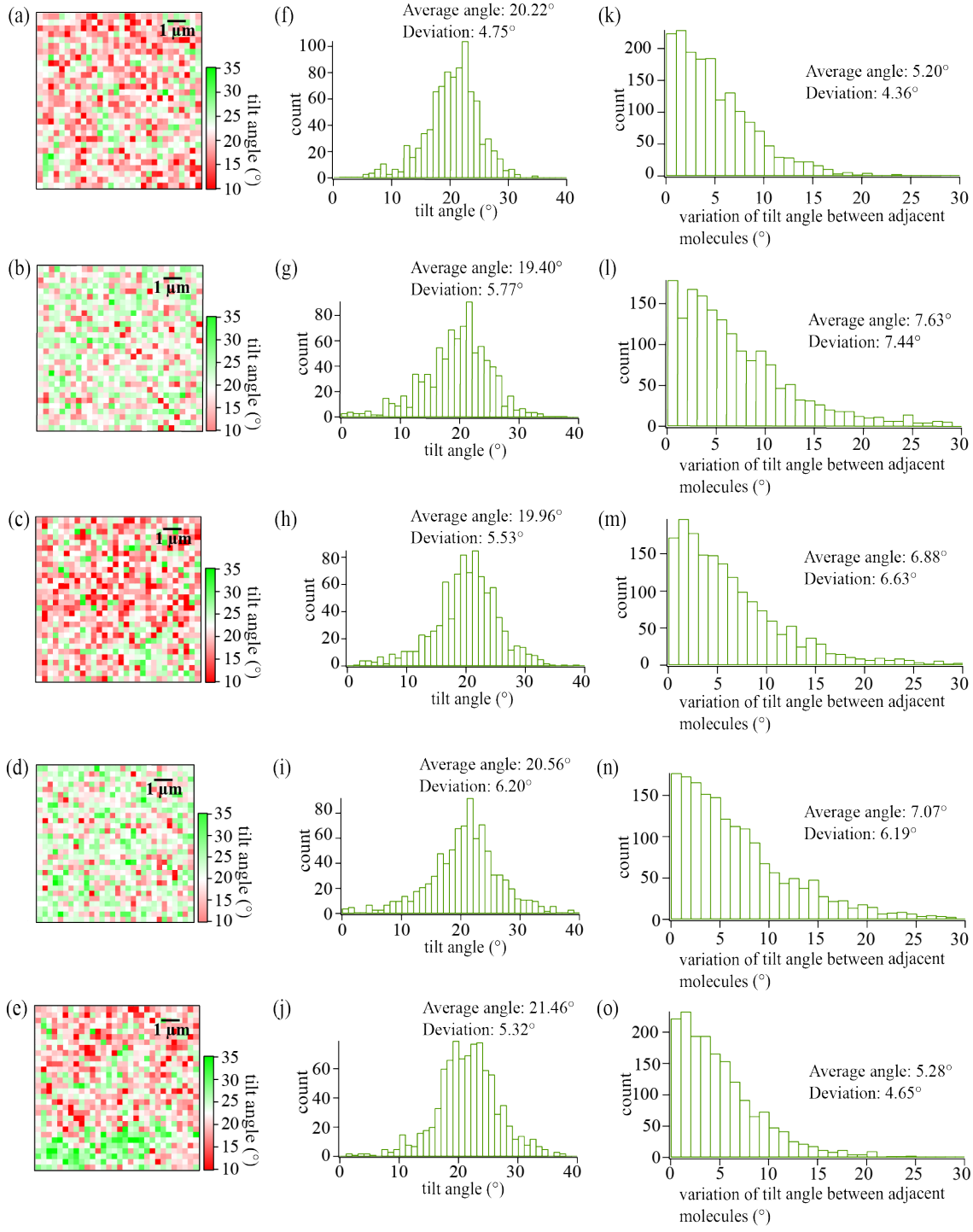


Figure 4-9. (**a**)-(**e**) show the molecular orientation distribution at five different regions of the non-sublimated pentacene transistor device. Histograms (**f**)-(**j**) show the corresponding tilt angle variation for the same five positions, and histograms (**k**)-(**o**) show the difference of the tilt angle between adjacent positions that is separated by few hundreds of nanometers in the transistor device.

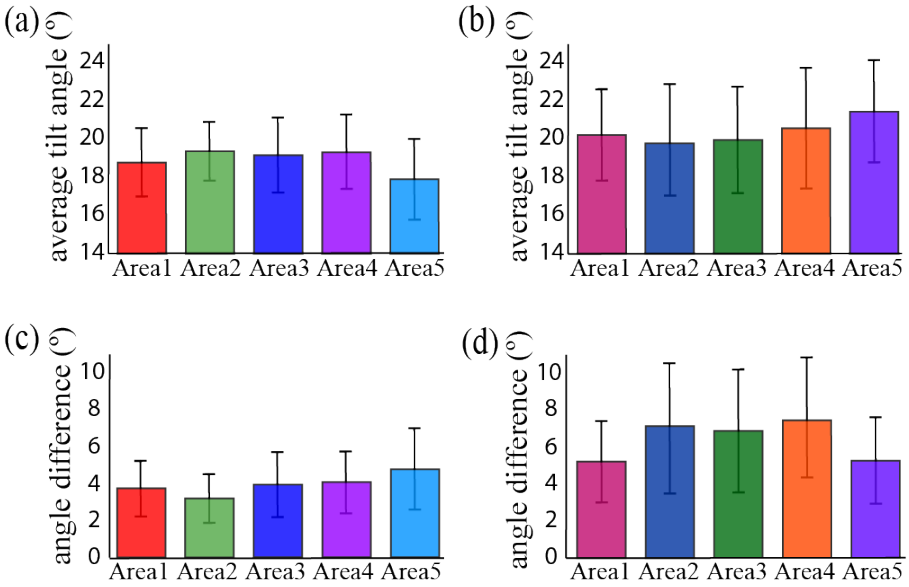


Figure 4-10. Bar graphs that show average of tilt angles at five different regions with their standard deviations for (**a**) sublimated and (**b**) non-sublimated devices, Average tilt angle difference between the neighboring positions in these regions for (**c**) sublimated and (**d**) non-sublimated devices.

The measurement areas in the device were separated by a distance of 10 µm from each other. Using bar graphs, the average tilt angle at five different regions of the sublimated and the non-sublimated device are represented in Figures 4-10(a) and 4-10(b), respectively, along with their standard deviations. The calculated values of average tilt angles were 18.78°, 19.36°, 19.16°, 19.34°, and 17.90° with standard deviations of ±3.53°, ±3.05°, ±3.89°, ±3.87°, and ±4.18°, respectively, at the five different regions of the sublimated device. Also, these values for the non-sublimated device were 20.22°, 19.40°, 19.96°, 20.56°, and 21.46° with standard deviations of ±4.75°, ±5.77°, ±5.53°, ±6.20°, and ±5.32°, respectively, at five different regions of the device. Hence, the sublimated device shows a smaller tilt angle with small deviations than those of

non-sublimated device. Further, I calculated tilt angle differences between the neighboring positions in these devices, which are shown in Figures 4-10(a) and 4-10(b). This show that pentacene molecules in sublimated device are well aligned in wider area that contribute to its high carrier mobility.

Conclusion

This work report on molecular orientation distributions of organic molecule pentacene in fabricated devices using polarization-based Raman spectroscopy. The carrier mobility of a transistor device is affected by the orientation angles of pentacene molecules. Fabricated pentacene sublimated and non-sublimated transistors devices show a considerable difference between them. Even though, surface morphologies of pentacene molecules in two types of fabricated devices appeared similar by the atomic force microscopy (AFM) analysis, average tilt angle and the tilt angle differences between neighboring regions in the device were smaller for the sublimated device compared to that of the non-sublimated pentacene transistor device. Several measurements were done in wider regions of both devices, which show smaller values of average tilt angle and tilt angle differences with small deviations in all measured areas of the sublimated device in comparison to those of non-sublimated device. These results confirm that the pentacene molecules in the sublimated device were well aligned over wider areas of the device that reflects in its high carrier mobility. This information could be crucial for further improving the performance of the transistor device.

References

1. Y.-Y. Lin, D. J. Gundlach, S. F. Nelson, and T. N. Jackson, IEEE Trans. Electron Devices. 44, 1325-1331 (1997).
2. T. W. Kelley et al. J. Phys. Chem. B 107, 5877-5881 (2003).
3. E. Gomar-Nadal, B. R. Conrad, G. C. William, and E. D. Willams, J. Phys. Chem. C 112, 5646-5650 (2008).
4. O. D. Jurchescu, J. Baas, and T. T. M. Palstra, Appl. Phys. Lett. 84, 3061-3063 (2004).
5. M. Shtein, J. Mapel, J. B. Benzinger, and S. R. Forrest, Appl. Phys. Lett. 81, 268-270 (2002).
6. D. Knipp, R. A. Street, A. Völkel, and J. J. Ho, Appl. Phys. 93, 347-355 (2003).
7. D. Knipp, R. A. Street, and A. R. Völkel, Appl. Phys. Lett. 82, 3907-3909 (2003).
8. R. Ruiz, A. Papadimitratos, A. C. Mayer, and G. G. Malliaras, Adv. Mater. 17, 1795-1798 (2005).
9. T. Mino et al., J. Raman Spectrosc. 43, 2029-2034 (2012).
10. K. Fukuda et al., Appl. Phys. Lett. 96, 053302 (2010).
11. Y. Saito, and P. Verma, J. Phys. Chem. Lett. 3, 1295-1300 (2012).

Chapter 5. Raman spectroscopic investigations of dinaphthothienothiophene (DNTT)

In this chapter, my research work on a fabricated transistor device using Raman spectroscopic studies of DNTT molecules be discussed. I will describe the structure and properties of the DNTT molecule and the fabrication of DNTT based transistor device in detail. Then, I will explain the Raman spectroscopic analysis of DNTT molecules using DFT calculation. I will also discuss the alignment of this molecule in the fabricated device using the polarization based Raman spectroscopy in this section.

5.1 Introduction of DNTT molecule

In this work, the organic semiconductor dinaphthothienothiophene ($C_{22}H_{12}S_2$, DNTT) that was developed by Yamamoto and Takimiya in 2007 has been utilized. The DNTT molecule is a symmetric heteroarene with six fused aromatic rings consisting of two naphthalene and two thiophene units, as shown in Fig. 5-1. It currently receives a lot of attention due to its high mobility and its excellent air stability.[1-11] For single-crystals of DNTT, Haas et al., reported mobility of 8.3 cm^2, and in polycrystalline thin-films, reasonably large hole mobility of 3 cm^2 was measured.[12]

The mobility of the charge carrier depends on the π- π interactions of adjacent DNTT molecules in the transistor devices. In order to get very high mobility in charge carrier, these molecules should be aligned and tightly packed in the device in such

fashion that organic aromatic rings of all DNTT molecules remain parallelly facing each other. In this condition, π-electrons interaction among adjacent molecules would be stronger that would contribute to the high transport of charge carriers. Therefore, I can expect the degraded performance of the device if DNTT molecules have a possible molecular twist and low molecular density that worsen the π - π overlapping between DNTT molecules. Thus, the molecular twist and density of DNTT molecules have a major effect on the device performance. Therefore, it is necessary to investigate these structural features in an actual fabricated transistor device, such studies will be helpful in improving the functioning of the device.

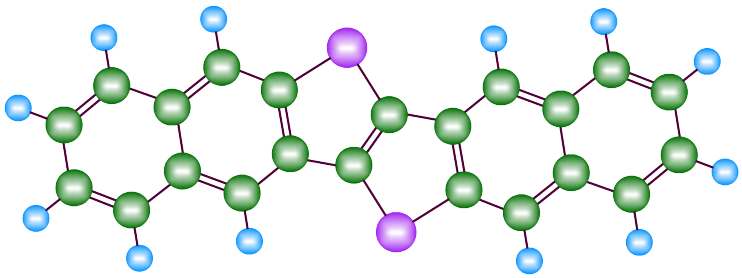


Figure 5-1. Molecular structure of the DNTT molecule. Green, blue, and Purple spheres represent carbon, hydrogen, and sulphur atoms, respectively.

5.2 Fabrication of transistor device based on DNTT

The DNTT based transistor device was provided by Prof. Sekitani's lab and measurement of electronic properties was also performed by the same group. Fig. 5-2

shows the schematic representation of fabricated device. In order to fabricate this device, first, a 30-nanometer thickness of Al layer was deposited on a glass substrate utilizing vacuum deposition (ULVAC EX-200). This thin layer is the gate of the transistor device. Then, the substrate was anodized in citric acid ($C_6H_8O_7$) having concentration of 1 millimolar that grow an aluminum oxide (AlO_x) layer over this substrate. Moving further, the substrate was immersed in 3 millimolar of dodecylphosphonic acid ($C_{12}H_{27}O_3P$) for 12 hours at 30°C that grows a dodecylphosphonate self-assembled monolayer (SAM) and then the substrate was rinsed in isopropyl alcohol and dry using the flow of the nitrogen gas. Here, the combination of AlO_x-SAM layer act as the gate dielectric of the transistor device. Over this substrate, a 30-nanometer thickness of DNTT organic molecules was deposited at the rate of 0.2 Å/s by the vacuum deposition that acts as the active region of the device. In the final step, a 50-nanometer thin gold layer was deposited through a shadow mask that defines the position of source and drains contacts on the device. This device was then annealed at 100°C for about 1 hour in vacuum. It was reported that the DNTT molecules grow perpendicular to the AlO_x-SAM substrate that means the long axes of DNTT molecules are in the normal direction to the substrate.[13] This molecular alignment of DNTT molecules can provide to high carrier mobility of the transistor due to the π-π overlapping between the adjacent molecules.

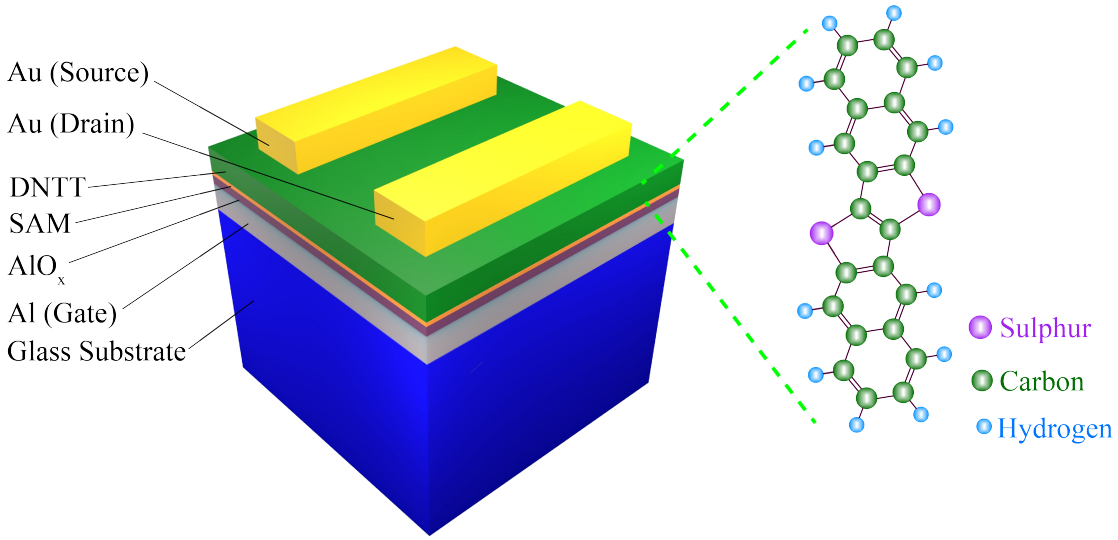


Figure 5-2. A schematic of the fabricated DNTT transistor device along with the structure of the DNTT molecule. Green, blue, and purple spheres represent carbon, hydrogen, and sulphur atoms, respectively.

5.3 Raman spectroscopic analysis of DNTT in a transistor device

I designed an optical set-up that works in the backscattered configuration for measuring the Raman spectrum of the DNTT molecule. The proposed schematic of the optical set-up is illustrated in Fig. 5-3(a). I used a 532 nm laser that is far from the absorption peak (445 nm) of DNTT molecules.[14,15] The incident laser was focused on the transistor device, which was kept in an inverted position at the sample stage, through an objective lens of magnification 150× and a numerical aperture of 0.95. The polarization of incident laser was controlled using a combination of a half-wave plate ($\lambda/2$ plate) and a linear polarizer. Same objective lens collects the Raman scattered signal from the device. This scattered signal was then dispersed using a spectrograph with a grating of 1800 grooves per mm, and then, detected with the help of a CCD camera. I used a notch

filter for blocking of Rayleigh light coming from the sample. Using this designed optical set-up, I measured the Raman spectrum of DNTT molecules, which is displayed in Fig. 5-3(b). The Raman spectrum shows multiple vibrational peaks in 1100 to 1650 cm^{-1} spectral range that is marked as peaks 1 to 13 in the spectrum. Further, I measured spectra in a 5 × 5 μm^2 area of the transistor device with 20 × 20 pixels by scanning the sample and constructed a Raman image using the intensity of the peak 10 observed at 1478.2 cm^{-1}. The Raman scattered signal depends upon the count of molecules that lie within the focal volume of the incident laser. Thus, the constructed Raman image, as shown in Fig. 5-3(c), represent the density distribution of DNTT molecules in the device. The strong Raman intensity regions in the image represent a high density of DNTT molecules whereas, weak Raman intensity regions represent a low density of DNTT molecules. Therefore, the density of DNTT molecules was not uniform in the fabricated device, which can degrade the performance of the device. I selected peak 10 for showing an example of a Raman image because of its high intensity in comparison to other observed Raman peaks. The Raman images constructed by other Raman peaks also show a similar distribution of DNTT molecules. Thus, I can understand the density distribution of DNTT molecules in a transistor device with a resolution of a few hundreds of nanometers that can utilize in improving the fabrication process of the device for better performance.

Several vibrational modes were observed in the Raman spectrum of DNTT molecules, I performed a DFT calculation to understand the vibrational properties of each vibrational mode. I utilized the Gaussian 09 package for calculation using a functional method of B3LYP and a basis set of 6-311G (d, p). The calculated Raman spectrum also shows multiple vibrational modes, as shown in Figure 5-3(b), which are

in good agreement with those results obtained through experimentally for DNTT molecules. I found some slight differences in the calculated and observed Raman spectra because the calculation was performed on a single isolated DNTT molecule, while the experiment was done on a thick layer of DNTT on the substrate. I assigned the numbers 1 to 13 to peaks observed in the DFT calculation by comparing the spectral patterns between the experiment and the calculation.

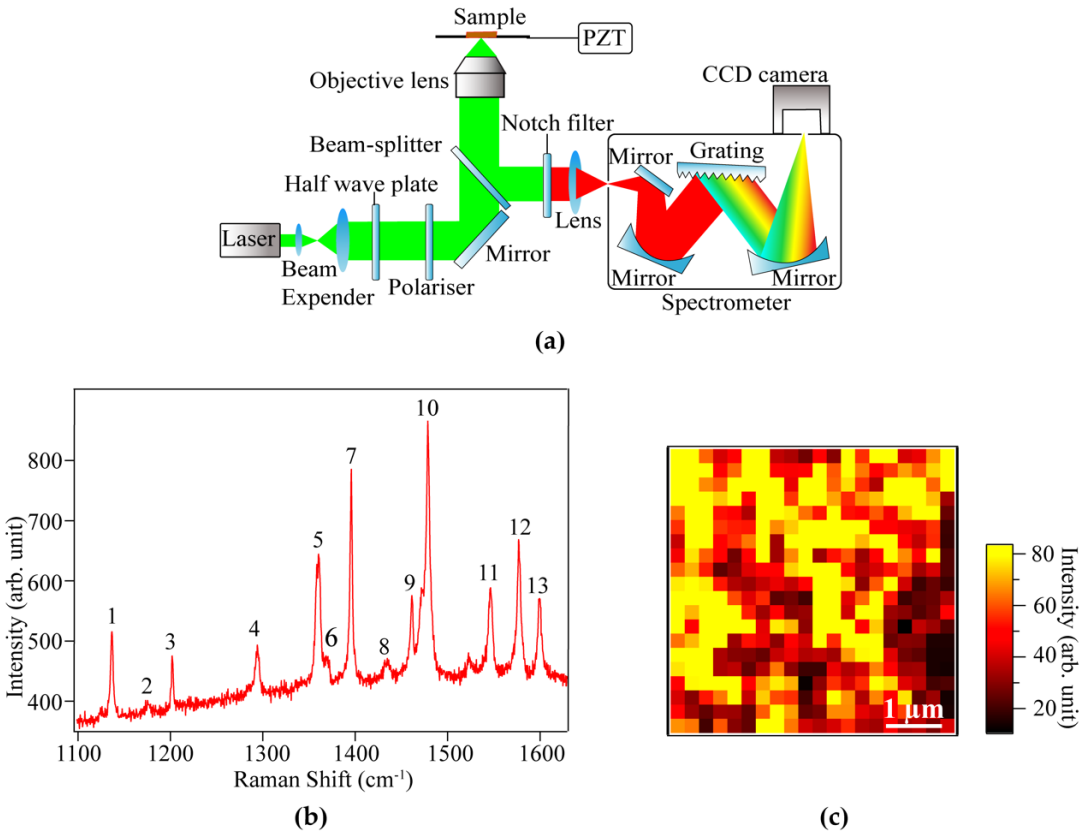


Figure 5-3. (a) A representation of the designed optical set-up, (b) a typical Raman spectrum of DNTT molecules measured with an exposure time of 30 s and an incident laser power of 140 µW, (c) Raman image of the transistor device constructed by the intensity of the peak 10.

From the results of the DFT calculation, I can understand the vibrational nature of each Raman mode with its vibrational strength and direction of molecular vibration. Figures 5-4(b) and 5-4(h) illustrate schematics of molecular vibrations related to several observed Raman peaks. In schematics, direction and length of the red arrows represent the direction and the strength of the molecular vibrations of the DNTT molecule. Here, I multiplied the initial length of all the arrows by a factor of 2.5 for their clear visualization. Also, I assigned each atom with a number over it for easy identification. The vibrational properties of each Raman peak can be easily understood and explained now. For example, I observed a strong C-C stretching of C(4) and C(9) carbon atoms in the case of peak 10, which was coupled with the C-H bending. In the case of peak 3, I observed C-H bending mode, where all hydrogen atoms in the lower part of the molecules bend in-phase. The bending of upper hydrogen atoms and lower hydrogen atoms were in anti-phase. In the case of peak 12, I observed deformation of all aromatic rings, whereas aromatic rings at both ends of the DNTT molecule mainly deforms in the case of a vibrational mode of peak 13. The vibrational modes of all the observed modes were originated from the combination of C-C stretching mode and C-H in-plane bending modes, and they have entirely different vibrational properties. I have summarized all the vibrational modes in Table 1.

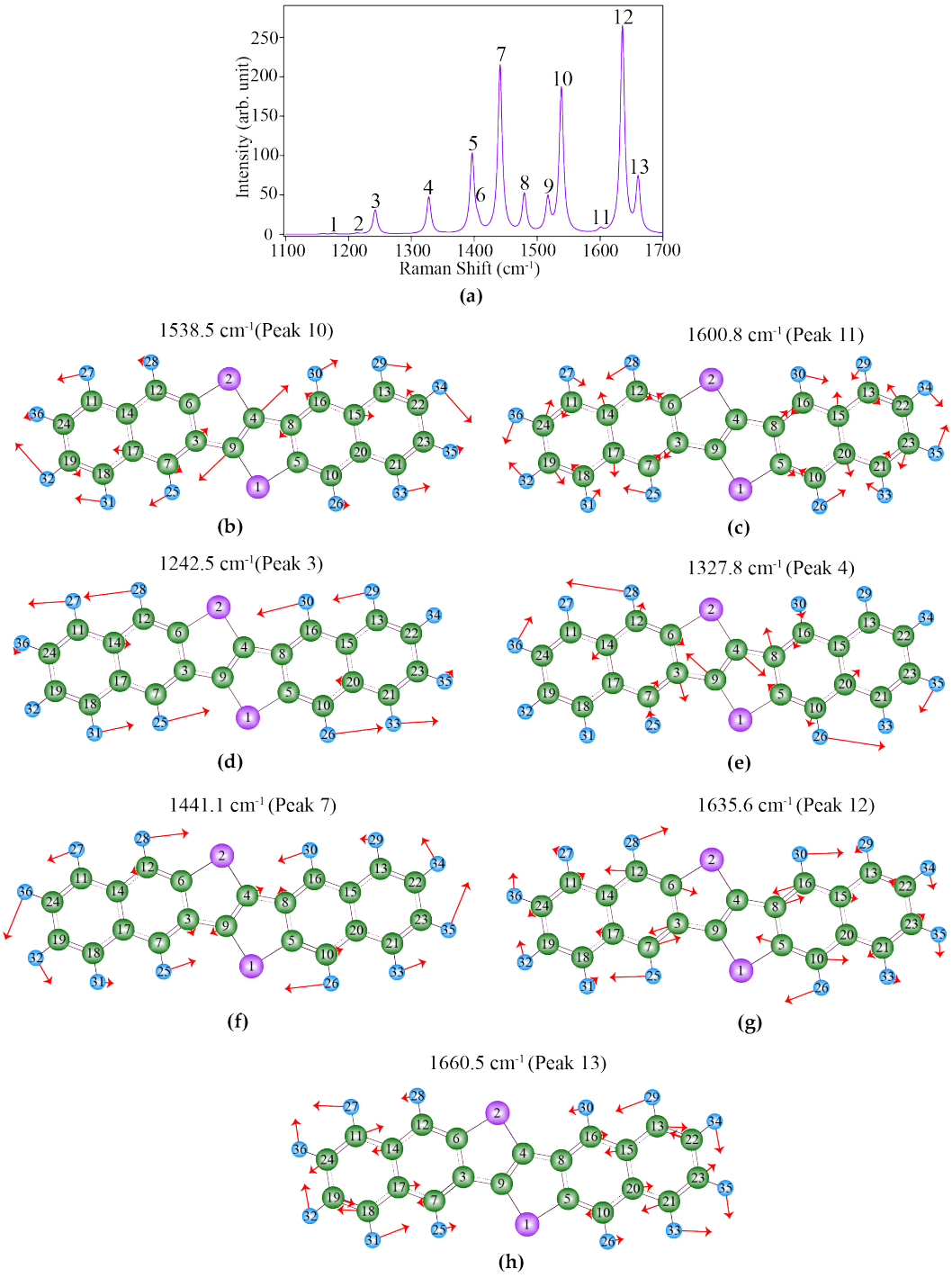


Figure 5.4. (a) A typical Raman spectrum of a DNTT molecule observed by the DFT calculation, graphical representations of molecular vibrations for (b) peak 10 and (c) peak11, (d) peak3, (e) peak4, (f) peak7, (g) peak12, and (h) peak13.

Table 1. Descriptions of the vibrations in the calculated vibrational modes.

Peak	Wavenumber (cm^{-1})	Descriptions
1	1176.5	C-H bending at the end of the aromatic rings
2	1213.9	C-H bending coupled with stretching of C(14), C(17), C(15) and C(20) atoms
3	1242.5	C-H bending; hydrogen atoms in the upper part of rings bend in-phase but hydrogen atoms in the upper and the lower parts bend anti-phase, and stretching of C(14) and C(20) atoms
4	1327.8	Deformation of thiophene rings and their adjacent aromatic rings and bending of H(26), H(28), H(35) and H(36) atoms
5	1396.7	C-C anti symmetric stretching of aromatic rings coupled with C-H bending
6	1405.8	C-C stretching coupled with C-H bending
7	1441.1	C-C symmetric stretching of aromatic rings coupled with C-H bending
8	1479.7	C-C stretching coupled with C-H bending
9	1517.0	C-C stretching coupled with C-H bending
10	1538.5	C-C stretching of the ring with a strong stretching of C(4)-C(9) atoms and C-H bending
11	1600.8	C-C symmetric stretching of the rings coupled with C-H bending
12	1635.6	Deformation of aromatic rings
13	1660.5	Deformation of the aromatic rings except for thiophene rings

As mentioned, the vibrational properties of all the observed modes were different from each other, which was understood by the DFT calculation. Among all vibrational modes, peak 11 shows a special vibrational property. Due to the stretching directions of carbon atoms, C(19)-C(24), C(17)-C(14), C(23)-C(22), and C(20)-C(15), the DNTT molecule appear to vibrate in the perpendicular direction of the long axis as shown in Fig. 5-4(c). The vibrational property of this mode is similar to the vibrational properties of similar molecule pentacene at 1533 cm^{-1}, which was reported as a polarization-dependent vibrational mode.[16] Therefore, I selected this vibrational mode for further investigations for the polarization dependence study. The unique property of this mode can be utilized

for the analysis of twist angles of DNTT molecules in the device through its polarization dependence. If I use an incident light whose polarization is in the direction of the C-C stretching, then the vibration amplitude of the DNTT molecule would enhance after interaction with incident light. As a result, the Raman intensity of peak 11 would also be enhanced. On the other hand, if the polarization direction of incident light would be in the perpendicular direction of the C-C stretching, then Raman intensity would reduce. Thus, the ratio of intensities under the known polarizations direction would give the relevant information about the twist angle of standing DNTT molecules.

Further, I estimated the twist angles of standing DNTT molecules using the polarization dependence of vibrational mode at the peak 11. The linear polarization directions of incident light were monitored with the help of a half-wave plate and a linear polarizer in the optical set-up. I generated two orthogonal linear polarizations of the incident light, whose directions were parallel to the transistor device plane. If I say the direction of the molecular axis of the standing DNTT molecule as z-direction, then the incident laser was polarized within the xy-direction, as shown in Fig. 5.5 using doubled sided green arrows. In my previous work, which is described in chapter 4, I utilized two mutually perpendicular polarizations, one was along the xy-plane, and the other was in the direction of the z-axis. Thus, the ratio of Raman intensities for this two polarizations gives basic information about the tilt orientation angle of pentacene. On the other hand, in the present case, both the polarization directions were in xy-plane, which is different from the previous case. Here, it is known that the DNTT molecules are stand along the z-direction on the AlO_x-SAM substrate. However, they can also

have twist while standing on this substrate. Therefore, if I use two mutually perpendicular polarizations of the incident light, both have polarization direction in xy-plane, then these provide information about the twist orientation angle of the standing DNTT molecule on the substrate. As shown in Fig. 5-5, if one of the polarization in the direction of vibrations of molecules, then Raman intensity would be maximum. On the other hand, if polarization direction is perpendicular to the molecular vibrations, then Raman intensity would be minimum. Therefore, the ratio of Raman intensities under these two polarizations measured at the same position would give relevant information about the twist orientation angle of DNTT molecules.

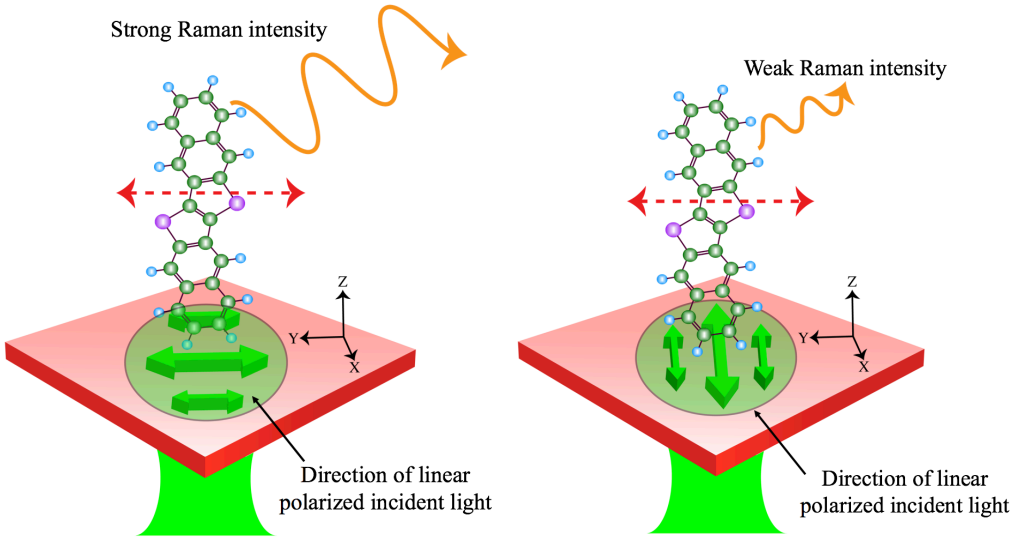


Figure 5.5. Molecular orientation analysis of DNTT with linear polarization incident light

Figure 5-6(a) shows Raman spectra measured at the same position of the device by two mutually perpendicular polarization of incident light. I observed a change in intensity of

peak 11, which confirms the polarization dependence of this peak. Further, I measured Raman spectra in a 7.5 × 7.5 μm^2 area of the transistor device with 25 × 25 pixels and constructed a Raman intensity ratio image of peak 11, as shown in Fig. 5-6(b), under these two incident polarizations. The variation of the twist angle of standing DNTT molecules in the device can be seen through the color variation in this image. The image also indicates that there are large areas of the device where the uniform twist of the molecules observed, and hence, I expect good transportation of charge carriers in this region that can be interrupted by the variation of color with different twist angles in the device. Thus, I observed that the distribution of twist angle of DNTT molecules was not homogeneous in the transistor device using the polarization-dependent Raman spectroscopic technique, as shown by a 3D illustration in Fig. 5-6(c). This information can help improving the performance of the transistor device by tweaking the growth parameters of DNTT molecules.

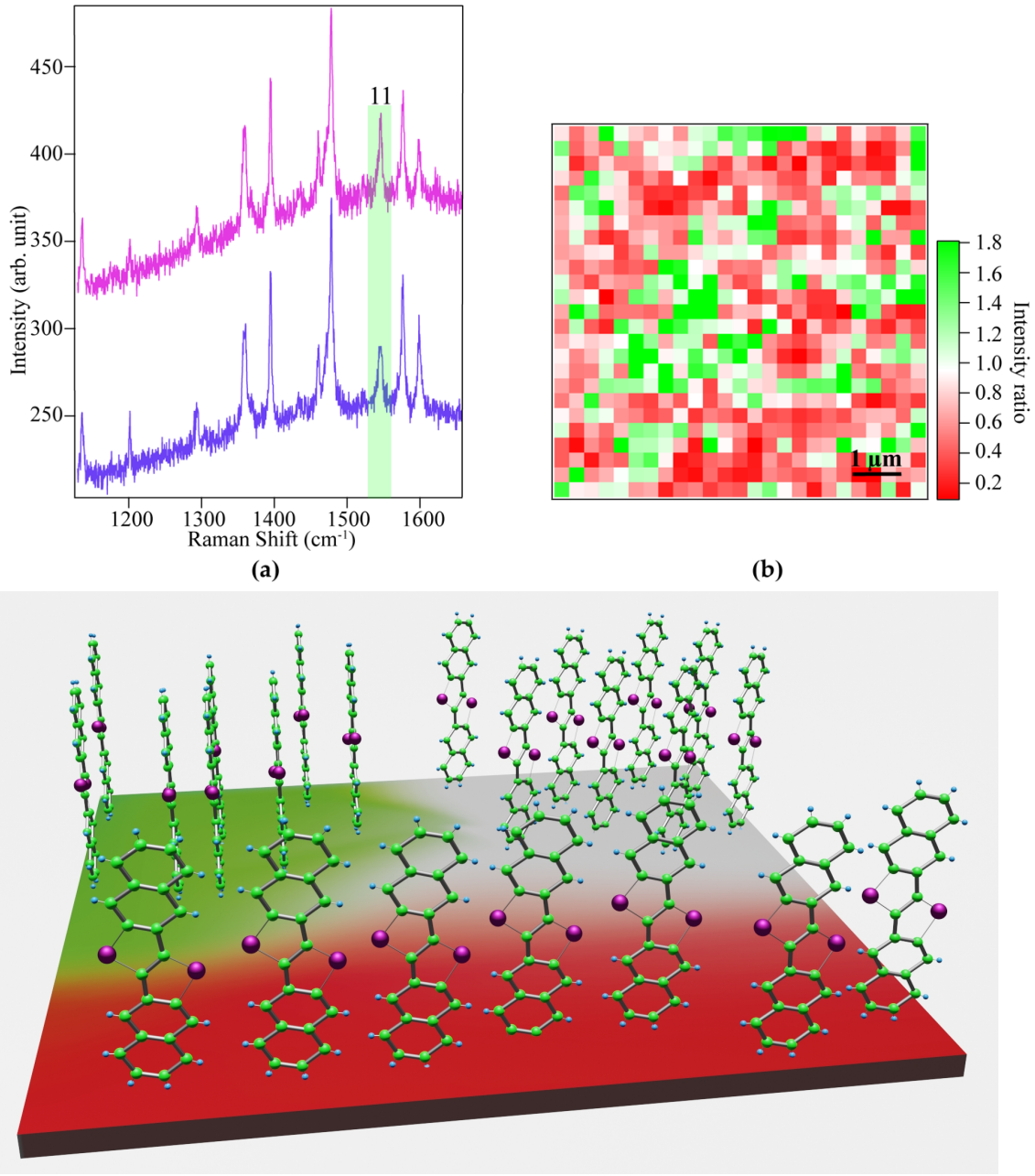


Figure 5.6. (**a**) Polarization-dependent Raman spectra measured with two mutually perpendicular linear polarization of incident light; (**b**) Raman intensity ratio image shows the distribution of orientation of DNTT molecules, (**c**) A 3D illustration of molecular orientation of DNTT molecules.

Conclusions

I investigated the Raman measurements of the DNTT molecule in a transistor device for the first time. Multiple vibrational modes were observed in the Raman spectrum of DNTT molecules. DFT calculation was used to analyze the nature of these mode vibrations. I investigated the density of DNTT molecules in the device using Raman imaging, and I found the density distributions were not homogeneous. The peak 11 shows dominant vibrations of the molecule in a specific direction. By taking advantage of this vibrational mode, I investigated the twist angle of the DNTT molecule using two mutually perpendicular linearly polarized beam. The orientation distributions of DNTT molecules were studied, and I found the distributions were not uniform in the transistor device. This information can be utilized in improving the performance of the device made of DNTT.

References

1. J. A. Rogers, Z. Bao, K. Baldwin, A. Dodabalapur, B. Crone, V.R. Raju, H. Kuck, H. Katz, K. Amundson, J. Ewing, and P. Drzaic, Proc. Natl. Acad. Sci, 98, 4835–4840 (2001).
2. F. Eder, H. Klauk, M. Halik, U. Zschieschang, G. Schmid, and C. Dehm, Appl. Phys. Lett., 84, 2673-2675 (2004).
3. B. K. Crone, A. Dodabalapur, R. Sarpeshkar, R. W. Filas, Y. –Y. Lin, Z. Bao, J. H. O'Neill, W. Li, and H. E. Katz, J. Appl. Phys., 89, 5125–5132 (2001).
4. T. Someya, Y. Kato, T. Sekitani, S. Iba, Y. Noguchi, Y. Murase, H. Kawaguchi, and T. Sakurai, Proc. Natl. Acad. Sci. 102, 12321–12325 (2005).
5. H. E. Katz, Z. Bao, and S. L. Gilat, Acc. Chem. Res., 34, 359–369 (2001).
6. J. E. Anthony, Chem. Rev., 106, 5028–5048 (2006).

7. Y. Lin, D. J. Gundlach, S. F. Nelson, and T. N. Jackson, IEEE Trans. Electron Devices, 44, 1325–1331 (1997).
8. T. W. Kelley, L. D. Boardman, T. D. Dunbar, D. V. Muyres, M. J. Pellerite, and T. P. J. Smith, Phys. Chem. B, 107, 5877–5881 (2003).
9. A. Maliakal, K. Raghavachari, H. Katz, E. Chandross, and T. Siegrist, Chem. Mater., 16, 4980–4986 (2004).
10. Y. Natsume, Phys. status solidi, 205, 2958–2965 (2008).
11. T. Yamamoto, and K. Takimiya, J. Am. Chem. Soc., 129, 2224–2225 (2007).
12. U. Zschieschang, R. Hofmockel, R. Rödel, U. Kraft, M. J. Kang, K. Takimiya, T. Zaki, F. Letzkus, J. Butschke, H. Richter, J. N. Burghartz, and H. Klauk, H. Org. Electron., 14, 1516–1520 (2013).
13. T. Breuer, A. Karthäuser, H. Klemm, F. Genuzio, G. Peschel, A. Fuhrich, T. Schmidt, and G. Witte, ACS Appl. Mater. Interfaces, 9, 8384–8392 (2017).
14. M. J. Kang, I. Doi, H. Mori, E. Miyazaki, K. Takimiya, M. Ikeda, and H. Kuwabara, Adv. Mater., 23, 1222–1225 (2011).
15. J. Milvich, T. Zaki, M. Aghamohammadi, R. Rödel, U. Kraft, H. Klauk, J. Burghartz, J. N. Org. Electron., 20, 63–68 (2015).
16. Y. Hosoi, D.M. Deyra, K. Nakajima, and Y. Furukawa, Mol. Cryst. Liq. Cryst., 491, 317–323 (2008).

Chapter 6. Investigation of the intermolecular interactions of Dinaphthothienothiophene (DNTT) molecules in a transistor device by low-frequency Raman spectroscopy

In this chapter, I discuss my work on low-frequency Raman spectroscopic studies of intermolecular interactions of DNTT molecules in an actual transistor device. Firstly, I introduce the low-frequency Raman spectroscopy and then, I discuss an experimental setup for measuring low-frequency Raman modes. Finally, I discuss the investigation of the intermolecular interactions of DNTT, which arise due to the molecular proximity, in the device.

6.1 Introduction of the low-frequency Raman spectroscopy

Low-frequency Raman modes refers to the vibrational modes that exist in the low Raman shift region, which is close to the Rayleigh line of the incident laser. They arise due to weak van der Waals interactions among the molecules and hence, these modes have weak oscillation energies and appear in the low-frequency range of Raman spectrum. In Raman measurement, vibrations of the molecules are distinguished by two kinds of vibrational modes, internal vibrations mode, and external vibrations mode. The internal vibrations mode arises due to the vibrations of atoms within the molecule, whereas the intermolecular interactions between the neighboring molecules are responsible for the external vibrations mode. The high-frequency Raman regions, also called the fingerprint region of Raman spectra, are mainly used in analyzing the internal

molecular vibration and internal molecular bonding of molecules within samples. Since low-frequency Raman spectra exhibit characteristics attributing to external vibrations of the molecules, they are used in various applications, such as polymorph identification and detection, material structure and phase determination, and identification of different drugs and protein.[1-6] The low-frequency Raman modes would give information about the intermolecular interactions, which are van der Waals in nature.[7] These interactions of organic molecules occur due to their proximities, and these proximities help in enabling a good flow of charge carriers in the transistor device. Therefore, the performance of the device depends upon the proximities of the molecules within the device. Thus, a study of the intermolecular interaction using the low-frequency Raman spectroscopy is important because it could help in further improving the device performance.

The detection of the low-frequency Raman signal is challenging as it requires efficient blocking of the Rayleigh scattered light that makes it difficult to detect the low-frequency Raman signal. So far, optical filers such as edge filter and notch filter are used to block Rayleigh scattered light. Edge filter is a long-pass filter that used to pass above a specific wavelength of the incident light. On the other hand, a notch filter is used to absorb a specific wavelength of the excitation light. Therefore, the Rayleigh scattered light will be absorbed, and the Raman signal above or below the Rayleigh light will be transmitted using a notch filter. Although these kinds of filters can block the Rayleigh scattered light, the minimum range of detecting Raman shifts cannot be reduced below to 100 cm^{-1}, as shown in Fig. 6-1. For example, low-frequency Raman

signals of an organic molecule anthracene lie close to the Rayleigh line, and it would not be very easy to observe these signals with normal filters due to their inability to block the broad Rayleigh scattered light as shown in the green color region in Fig. 6-1.

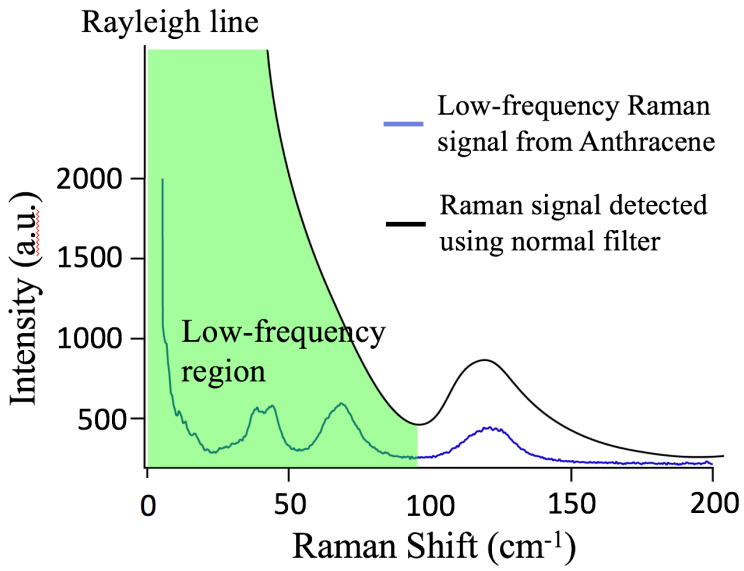


Fig. 6-1. Illustration of Raman signal detected using a normal filter and a typical low-frequency Raman spectrum of Anthracene.

There are some methods to detect low-frequency Raman signals from a sample. Traditionally, a triple monochromator instrument was used to detect low-frequency Raman signals coming from a sample. The first two monochromators in this instrument used to block the Rayleigh scattered light physically, and the third spectrometer then acts in a usual way to disperse the Raman scattered light for detection using CCD camera. Since this technique requires signals to pass through three spectrometers, the throughput of the detected signal becomes low. Also, this instrument does require more

expertise to be operated in comparison with the instrument using a normal filter in single spectrometer systems. Therefore, this instrument would rarely be considered for measuring low-frequency Raman signals of a sample. In my research, I have used three Bragg notch filters in my experimental set-up, which helped me in detecting Raman signals down to 10 cm^{-1}. The Bragg notch filter is a volume Bragg grating, which is recorded in the photosensitive material. It reflects the incident light with bandwidth as narrow as 4 cm^{-1}, when the Bragg condition is satisfied. I measured low-frequency Raman signal coming from the DNTT molecules using the designed experimental set-up.

6.2 Experimental setup for low-frequency Raman spectroscopy

The low-frequency Raman spectrum of the DNTT molecule was measured by utilizing a backscattering configuration of an optical set-up, as shown in Fig. 6-2(a). Here, the DNTT based transistor device was fabricated using the same procedure as mentioned in chapter 5 for pentacene transistor device, and the measurement was performed in the regions between drain and source contacts of the device. I used a circular polarization of incident light with a wavelength of 532 nm, which is generated by using a half-wave plate ($\lambda/2$ plate), a linear polarizer, and a quarter-wave plate ($\lambda/4$ plate) in the optical path of incident light. The incident circularly polarized light helps in avoiding any polarization dependence of any Raman vibrational mode on the incident laser excitation. I used an objective lens of 150× magnification and 0.95 numerical

aperture to focus the laser on the device, then the same objective lens was used in collecting Raman scattered signals coming from the device. The collected Raman scattered light was dispersed with the help of a spectrometer with a grating of 1200 grooves per mm, and detected using a CCD camera. To detect the low-frequency Raman signal, I utilized three Bragg grating notch filters (B1, B2 and B3) (OptiGrate, Orlando, FL, USA) in output of optical path, which enables the instrument to detect Raman signal from DNTT molecules down to 10 cm^{-1}.

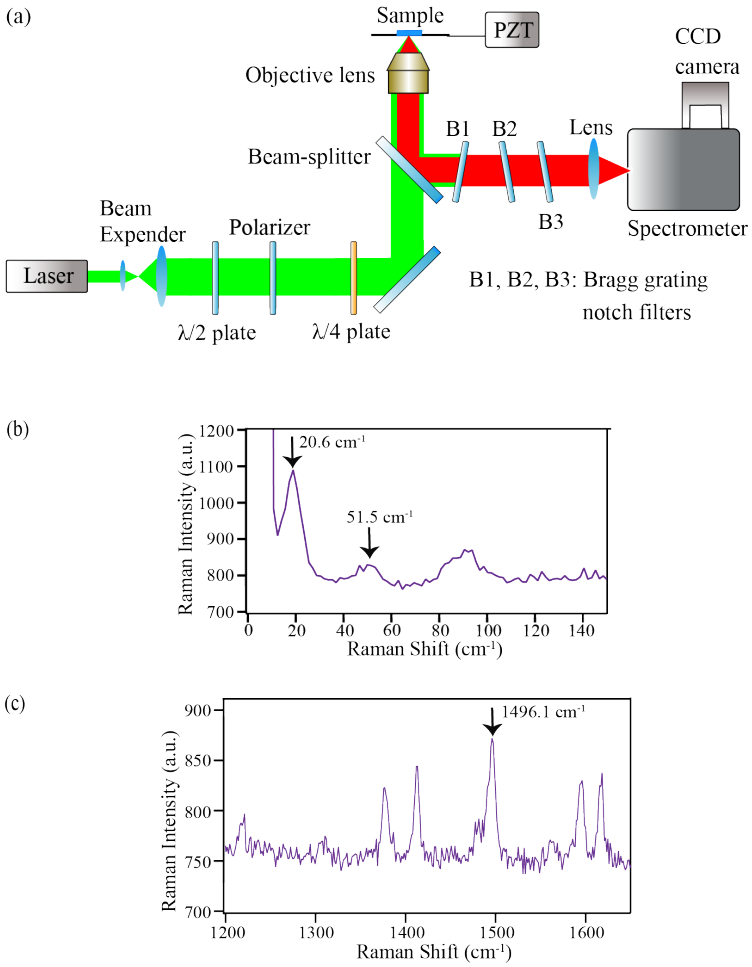


Fig. 6-2. (a) Experimental set-up for measuring the low-frequency Raman spectrum, (b) a low-frequency Raman spectrum, (c) a high-frequency Raman spectrum of DNTT molecules.

6.3 Investigation of intermolecular interactions of DNTT in a transistor device

Firstly, I measured the Raman signal of the DNTT molecule that is displayed in Fig. 6-2(b). I used an exposure time of two seconds with laser power of 140 μW for this measurement. The observed low-frequency Raman spectrum that has peaks at 20.6 and 51.5 cm^{-1}. In comparison to other observed Raman peaks, the peak present at 20.6 cm^{-1} has a higher signal-to-noise ratio. Therefore, I choose this peak for my further study. I also measured a high-frequency Raman spectrum together with the low-frequency Raman spectrum in the same position, which is shown in Figure 6-2(c). In order to investigate further, I measured Raman spectra in a 10 × 10 μm^2 area of the transistor device with 32 × 32 pixels by scanning the device within the focus of the incident laser and constructed Raman images. I utilized intensity of the low-frequency and the high-frequency peak at 20.6 cm^{-1} and 1496.1 cm^{-1}, respectively for constructing a low-frequency and a high-frequency Raman image. These Raman images are shown in Figures 6-3(a) and 6-3(b). It is known that the high-frequency Raman image shows the density of DNTT molecules.[8] As the scattered Raman signals of low-frequency vibrational mode depend on the molecules that interact with one another, the Raman image created by low-frequency peak would give information about the interactions between the molecules together with the density information of DNTT molecules. Hence, the information about intermolecular interactions can be obtained by the division of the intensity of low-frequency vibrational mode to the high-frequency

vibrational mode in the same position. Figure 6-3(c) represents an image, which is constructed from the intensity ratio of low-frequency to the high-frequency Raman intensity at various positions in the device. Before taking intensity ratio, I normalized both obtained images with their average intensity values in the measured region because these two Raman modes have varying intensities in this measured region. In Fig. 6-3(c), the ratio value of one indicates regions where the intensity of these two Raman modes are equal that would help in comparing both Raman images. Thus, variations in color in Fig. 6-3(c) represents how the intermolecular interactions are spatially distributed in the transistor device.

The image, displayed in Fig. 6-3(c), indicates that a strong intermolecular interaction in the red color areas as compared to the blue. Therefore, this indicates a larger interaction between the molecules in red color areas when compared to the molecules in blue color areas. The reason for the weak intermolecular interactions in the blue color regions could be due to the different orientations of adjacent DNTT molecules or a far separation of DNTT molecules from each other within the device. Therefore, I expect that the blue color regions would have degraded carrier mobility than the regions indicated in the red color. Thus, my measurement method gives information regarding the intermolecular interactions among DNTT molecules that affect the device performance. These findings will help in improving the performance of electronic devices made of DNTT molecules.

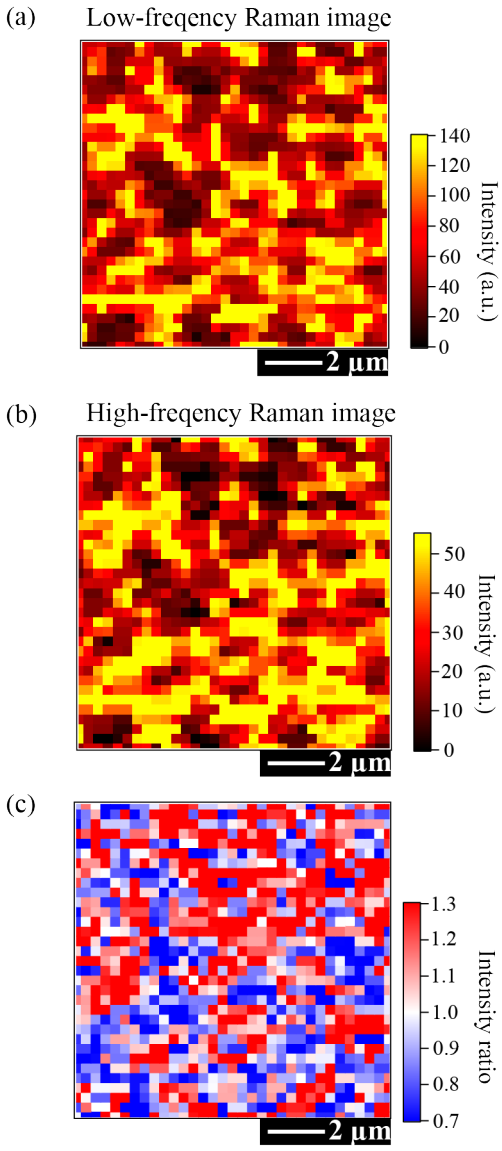


Fig. 6-3. A Raman map of DNTT molecules in a transistor device using (a) A low-frequency Raman mode, and (b) a high-frequency Raman mode. (c) a Raman intensity ratio image.

Conclusion

I designed an experimental setup to measure low-frequency Raman modes of DNTT molecules. I utilized three Bragg grating notch filters, which block incident light

efficiently, for detecting low-frequency Raman modes. I observed that DNTT molecules display a few low-frequency Raman peaks. The low-frequency Raman spectroscopic system with high detection efficiency further helped me to perform Raman imaging of DNTT molecules within the device. I found also that there is a variation in the spatial distribution of intermolecular interactions, i.e., the molecular packing, at a high spatial resolution in the fabricated transistor device. I also detected areas in the device that could have higher carrier mobility than the other regions of the device with a high spatial resolution. These findings can be utilized in further improvement in device performance.

References

1. B. S. Bhardwaj, T. Sugiyama, N. Namba, T. Umakoshi, T. Uemura, T. Sekitani and P. Verma, Sci. Rep. 12, 615 (2019).
2. Z. Shen, T. Yu, Y. Wang, and Z. Ni, Nano Res. 1, 273 (2008).
3. R. G. D. Valle, E. Venuti, L. Farina, and A. Brillante, J. Phys. Chem. B 108, 1822 (2004).
4. A. Girlando, M. Masino, A. Brillante, T. Toccoli, and S. Iannotta, Crystals 6, 41 (2016).
5. P. J. Larkin, M. Dabros, B. Sarsfield, E. Chan, J. T. Carriere, and B. C. Smith, Appl. Spectrosc. 68, 758 (2014).
6. M. Inoue, H. Hisada, T. Koide, J. Carriere, R. Heyler, and T. Fukami, Org. Process Res. Dev. 21, 262 (2017).

7. D. Tuschel, Spectroscopy 30, 14 (2015).
8. B. S. Bhardwaj, T. Sugiyama, N. Namba, T. Umakoshi, T. Uemura, T. Sekitani and P. Verma, Materials 12, 615 (2019).

Conclusions

Organic field-effect transistors (OFETs) has established itself as an important device for their use in electronics devices, such as non-volatile plastic memories, flexible digital screens, and sensors. Among various organic materials, pentacene and dinaphthothienothiophene (DNTT) have been widely investigated as a promising material for OFET devices owning to their high charge carrier mobility in the transistor device. Molecular structures of these molecule significantly affect the charge carrie mobility, knowing the various affecting factors such as orientations and density distribution would be of immense importance. Raman spectroscopy is an established tool to examine the structural properties of organic molecules with a reasonably high spatial resolution.

In this dissertation, I have in-depth studies the distribution of molecular orientation for pentacene organic molecules in a fabricated transistor device using polarization-based Raman spectroscopy technique. The presence of impurities in pentacene during fabrication of transistor device changes the molecular orientation of pentacene molecules thereby changing it transport properties of charge carriers. Sublimation is a well-known process to remove these impurities. In my work, I mapped the variation of molecular orientation between neighboring measurement positions that are spanned within a few hundreds of nanometers in fabricated transistor devices applying the sublimated and the non-sublimated pentacene, which can be directly correlated to the device performance and can be utilized in improving the performance

of the device. Also, I investigated the Raman spectroscopic studies on DNTT in an OFET device for the first time, which was further analyzed by the density functional theory (DFT) calculation. Besides these research works, I also investigated the Raman mapping of DNTT molecule with low frequency in a fabricated transistor device. Detection of low frequency Raman signal from DNTT molecules requires me to use several Bragg grating notch filters in my optical setup to efficiently block the laser light. It was observed for the first time that DNTT molecules show few low-frequency Raman peaks. The designed low-frequency Raman spectroscopic system with a high detection efficiency further enabled me to perform low-frequency Raman imaging of DNTT in the device. I found that there is a spatial variation of intermolecular interactions, i.e. the molecular packing, at a spatial resolution of a few hundreds of nanometers. This research work help in getting further insight into the performance of DNTT based transistor devices and contribute to the scientific knowledge about the understanding of the intermolecular interactions of DNTT molecules in electronic devices. Together with Raman spectroscopic technique which offers the advantage of being non-invasive, non-destructive and with high spatial resolution it can be used to further improve the performance of electronic devices made with DNTT molecules.

List of publications

Original papers

1. Bishwajeet Singh Bhardwaj, Rhea Thankam Sam, Takayuki Umakoshi, Naoko Namba, Takafumi Uemura, Tsuyoshi Sekitani and Prabhat Verma, "Probing inter-molecular interactions of Dinaphthothienothiophene (DNTT) molecules in a transistor device using low-frequency Raman spectroscopy", *Applied Physics Express*, **13**, 022010, (2020).
2. Bishwajeet Singh Bhardwaj, Takeshi Sugiyama, Naoko Namba, Takayuki Umakoshi, Takafumi Uemura, Tsuyoshi Sekitani and Prabhat Verma, "Orientation analysis of pentacene molecules in organic field-effect transistor devices using polarization dependent Raman spectroscopy", *Scientific Reports*, **9**, 15149, (2019).
3. Bishwajeet Singh Bhardwaj, Takeshi Sugiyama, Naoko Namba, Takayuki Umakoshi, Takafumi Uemura, Tsuyoshi Sekitani and Prabhat Verma, "Raman spectroscopic studies of Dinaphthothienothiophene (DNTT)", *Materials*, **12**, 615, (2019).

Conferences

1. Bishwajeet Singh Bhardwaj, Takeshi Sugiyama, Naoko Namba, Takayuki Umakoshi, Takafumi Uemura, Tsuyoshi Sekitani and Prabhat Verma, "Raman spectroscopic investigation of Dinaphthothienothiophene in a transistor device", Oral presentation, 66th Japanese Society of Applied Physics (JSAP) spring meeting, Tokyo institute of technology, Tokyo, Japan, March, (2019).
2. Bishwajeet Singh Bhardwaj, Takeshi Sugiyama, Naoko Namba, Takayuki

Umakoshi, Takafumi Uemura, Tsuyoshi Sekitani and Prabhat Verma, "Investigation of Dinaphthothienothiophene (DNTT) transistor device by Raman spectroscopy", Poster presentation, Global Nanophotonics, Tata Institute of Fundamental Research (TIFR), India, December, (2018).

3. Takeshi Sugiyama, Bishwajeet Singh Bhardwaj, Naoko Namba, Takayuki Umakoshi, Takafumi Uemura, Tsuyoshi Sekitani and Prabhat Verma, "Molecular orientation analysis in organic thin-film transistor device by polarized Raman microscopy", Poster presentation, SPIE Optics + Photonics, San Diego, USA, August, (2018).

ACKNOWLEDGEMENTS

This dissertation is the outcome of the valuable support and input of teachers, collaborators, friends, and family.

I would like to thanks my supervisor Prof. Prabhat Verma for his guidance, encouragement, and advices he has provided me all the time during my research. I have been extremely lucky to have such a supervisor who cared so much about my research work. I am thankful to him for answering my question promptly. He always inspired and helped me in pursuing a theoretical understanding of my research, developing writing paper skills, and making an effective presentation. I would like to again express my gratitude to him.

I also would like to express my sincere gratitude to Professor Takayuki Umakoshi for his valuable support. His calm and intellectual behavior gave me motivation towards my work. His suggestion always gave perfection in my research paper. Every time I talk to him about my research, and he always gave a new logic and guidance for my research. I am heartily thankful to him.

I am very thankful to Prof. Tsuyoshi Sekitani (The Institute of Scientific and Industrial Research, Osaka University), Prof. Takafumi Uemura (The Institute of Scientific and Industrial Research, Osaka University), and Dr. Naoko Namba for providing pentacene and DNTT samples that was helpful in pursuing my research.

I express my sincere thanks to Prof. Eiichi Tamiya (Department of Applied Physics, Osaka University), Prof. Yukihiro Ozaki (Department of Chemistry, Kwansei Gakuin University), and Prof. Yasushi Inouye (Department of Applied Physics, Osaka University) for giving valuable comments and beneficial suggestions that helped me to improve my work.

I appreciate NSOM group members, who helped in my research through daily discussion. Your unconditional all kinds of help made my research life pleasurable. I am flooded with beautiful memories with you all. I would like to thank Yoko Kanazawa for her support and making my lab life comfortable.

I finally give my sincere gratitude to my family and wife for their understanding, encouragement, support, and love throughout my life. It might be difficult to come this far without your support.